

# Implications of Transient Deformation in the Northern Basin and Range, Western United States

Ashutosh Chamoli<sup>1,2,\*</sup>, Anthony R. Lowry<sup>3</sup>, Tamara N. Jeppson<sup>4</sup>

<sup>1</sup>National Geophysical Research Institute, Council of Scientific & Industrial Research, Hyderabad, India

<sup>2</sup>Now at: Department of Earth Sciences, Indian Institute of Technology–Roorkee, Uttarakhand, India

<sup>3</sup>Department of Geology, Utah State University, Logan, Utah, USA

<sup>4</sup>Department of Geoscience, University of Wisconsin, Madison, Wisconsin, USA

Correspondence to: A. Chamoli (chamoli.a@gmail.com)

## Key Points

- GPS time series suggest transients coherently affect the entire province
- Quartz-rich crust and wet lithospheric column indicate Moho detachment unlikely
- Slip may activate discontinuous detachment surfaces near mid-crust

## Abstract

Transient deformation events observed in Global Positioning System (GPS) data from the Basin and Range extensional province may illuminate qualitatively similar transient events observed in subduction zones and other tectonic environments. We model GPS time series at twenty-two sites using a combination of hyperbolic tangent function analysis and elastic load deformation estimated from climatological data. We identify two transient events, ~2000.4 and ~2004.4, with roughly similar timing and displacement to those described previously by other researchers. The first few years of GPS observations, adopted as a reference state in earlier studies, are found to be anomalous. Our results differ from previous studies in two respects. First, a significant component of northward transient motion occurs during both events, despite a reversal of sign in east component motion. Second, sites move coherently in the eastern as well as the western Basin and Range. Surface mass loading, the largest source of transient stress forcing in the region, exhibits no evidence of a simple relationship to the deformation transients. Prior studies inferred slip on a single megadetachment at the Moho, but that hypothesis assumes negligible ductile deformation of the lower crust and a dry olivine rheology for the uppermost mantle. Recent measurements of crustal quartz abundance and effective elastic thickness suggest both assumptions are unlikely. Basin and Range transients can be reconciled with the frictional slip mechanism widely accepted for subduction zone transients provided that slip is occurring on discontinuous detachment surfaces at mid-crustal depths.

## 1. Introduction

The northern Basin and Range province is a broad, 300 to 800 km wide, intracontinental rift zone occupying a large fraction of the central Cordillera in the western United States (Figure 1). Extensional strain widened the central part of the province from ~30 to 14 Ma [e.g., *Dilles and Gans*, 1995], but extension has focused at the eastern and western margins since about 12 Ma [e.g., *Stockli et al.*, 2003; *Colgan et al.*, 2006]. Global Positioning System (GPS) geodetic measurements confirm that modern extensional strain continues to focus at the edges of the province in narrow, ~100 km wide zones [e.g., *Bennett et al.*, 2003; *Hammond and Thatcher*, 2004; *Berglund et al.*, 2012].

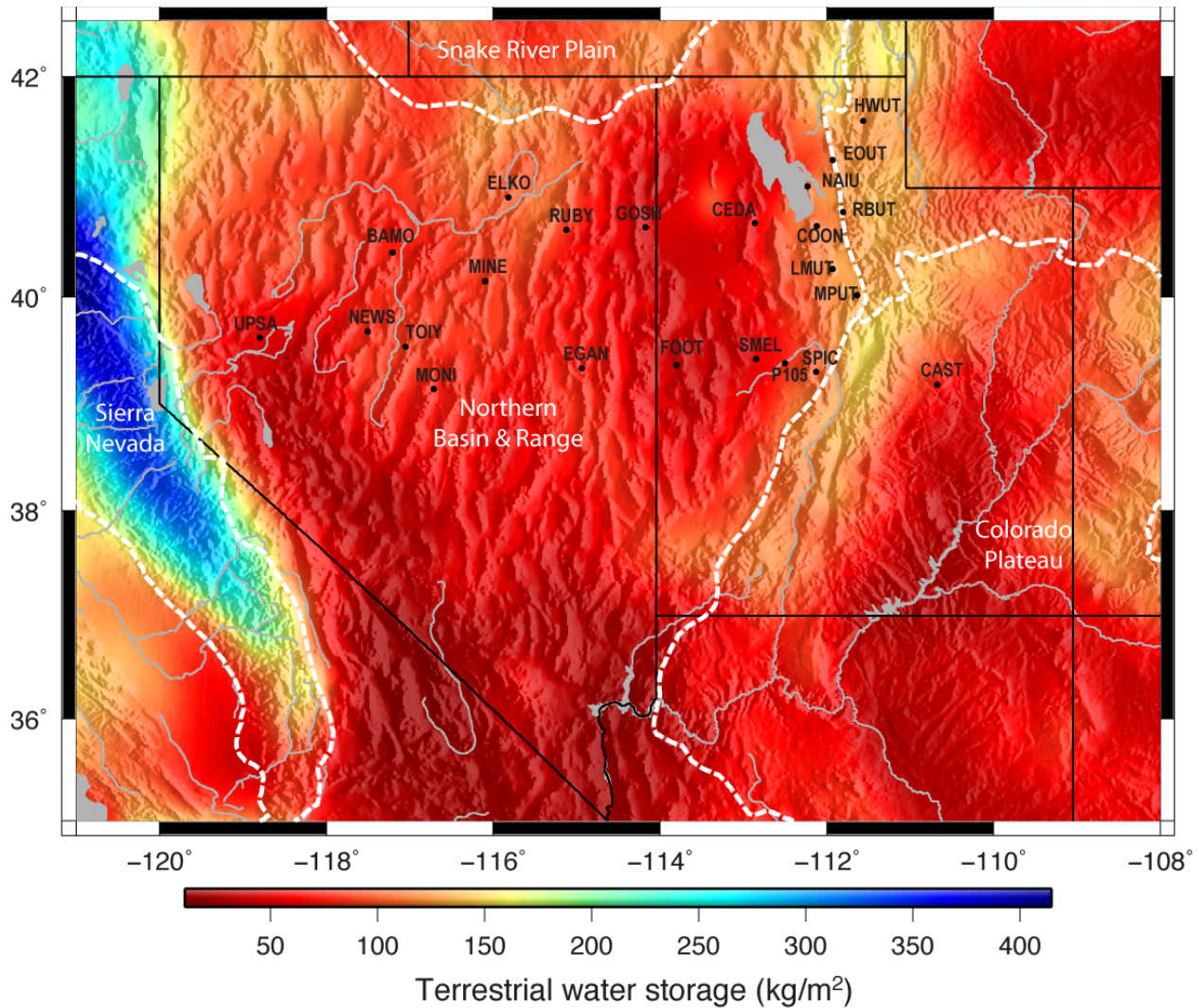


**Figure 1.** Location map of the northern Basin and Range province, including locations of GPS sites used in this analysis. Major lakes and rivers that contribute to surface hydrologic loading (but are unaccounted for in GLDAS L4 fields used here) are depicted grey; color contours (draped over topographic relief) reflect averaged peak-to-peak annual variation in hydrologic loading estimated from the GLDAS L4 land-surface climatological model.

An intriguing characteristic of the northern Basin and Range is that it does not extend at a constant rate. *Davis et al.* [2006] observed an approximate 1 mm/yr eastward perturbation of velocity in the western half of the Basin and Range from roughly 2000 to 2005. *Wernicke and Davis* [2010] examined Kalman-filtered velocity time series to infer two distinct, shorter eastward velocity perturbations across the western half of the province that peaked in 2000 and late 2003, with a westward anomaly in 2006, and an eastward anomaly in the eastern half of the Basin and Range also occurring around 2006.

Transient displacements in the Basin and Range are qualitatively similar to those observed during slow fault slip events, and they have been interpreted as evidence of transient frictional slip [*Davis et al.*, 2006; *Wernicke et al.*, 2008; *Wernicke and Davis*, 2010]. Slow slip events were first widely recognized from GPS measurements in subduction zones [*Hirose et al.*, 1999; *Dragert et al.*, 2001; *Lowry et al.*, 2001], and most subsequent observations of the phenomenon

have similarly been associated with subduction megathrusts [e.g., *Ohta et al.*, 2006, *McCaffrey et al.*, 2008; *Outerbridge et al.*, 2010]. Slow slip events have been observed from GPS data in other tectonic environments, however, including a low-angle thrust decollement flanking the Big Island of Hawaii [*Cervelli et al.*, 2002; *Brooks et al.*, 2008; *Foster et al.*, 2013]. Slow slip has been inferred on the San Andreas (California) and Alpine (New Zealand) strike slip faults from borehole strainmeter data [*Linde et al.*, 1996] and from observations of the tectonic tremor that commonly accompanies subduction zone slip events [*Nadeau and Dolenc*, 2005; *Wech et al.*, 2012].

Interpreting Basin and Range transient deformation as evidence of slow fault slip events is reasonable in the absence of obvious temporal variation in stress forcing, because most other rheological mechanisms lack the state variable needed to introduce temporal nonlinearity in the relationship of strain to stress forcing. However, invoking a rate- and state-dependent frictional mechanism also poses several challenging questions. For one, the region affected by coherent transient deformation is extremely broad, up to 500 km wide, leading to postulation of a subhorizontal megadetachment beneath the western Basin and Range of similar width [*Davis et al.*, 2006; *Wernicke et al.*, 2008]. Evidence of subhorizontal detachments exhumed from 10-15 km depths (once termed metamorphic core complexes) is ubiquitous across the Basin and Range [e.g., *Davis and Lister*, 1988; *Lister and Davis*, 1989; *Wernicke*, 1992; *Axen et al.*, 1993]. Some of these have mapped widths exceeding 50 km in the dip direction [e.g., *Howard and John*, 1987; *Axen and Fletcher*, 1998], and several were active as recently as 5-10 Ma, but observations do not support interpretation of a contiguous modern detachment surface of 300-500 km scale at depth.

Perhaps the most intriguing question however relates to depth of the deformation source. Subduction zone slow fault slip events often focus near the deep transition from velocity-weakening to velocity-strengthening friction at the base of the seismogenic zone [e.g., *Lowry*, 2006; *Ide et al.*, 2007; *McCaffrey et al.*, 2008; *Chapman and Melbourne*, 2010]. The maximum rupture depth for Basin and Range earthquakes is roughly 15 km [*Doser and Smith*, 1989], so if Basin and Range transient deformation is indeed similar to slow slip in subduction zones, the source should be in the midcrust. Studies of Basin and Range transients thus far have inferred a megadetachment at the Moho however [*Davis et al.*, 2006; *Wernicke et al.*, 2008; *Wernicke and Davis*, 2010], based on observations of strong reflection amplitudes there [*Hauser et al.*, 1987], the remarkably broad area activated during events, and temporal association with a lower-crustal magmatic intrusion event near the western edge of 2000-2004 transient deformation [*Smith et al.*, 2004].

The Moho detachment hypothesis assumes the uppermost mantle rheology is transitional between frictional and ductile, and that there is negligible crustal flow to decouple mantle from crustal deformation. *Wernicke et al.* [2008] cite several observations to support these assumptions, including low measured water content in nearby mantle xenoliths and a lack of evidence for crustal or uppermost mantle flow in rebound studies [*Bills et al.*, 2007; *Freed et al.*, 2007]. A ductile flow rheology is inferred at Moho depth from other lines of evidence, however, including seismic imaging of low relief [*Klemperer et al.*, 1986], textures of exhumed rocks [*Behr and Platt*, 2011], effective elastic thickness of the lithosphere [*Lowry et al.*, 2000], and dissimilarity of surface and Moho isostatic response to deep mass variations [*Seunarine and Lowry*, 2011].

In this study, timing and displacements of transients are estimated independently at twenty-two continuous GPS sites in the Basin and Range network using a modified hyperbolic tangent function analysis (HTFA). We remove hydrological mass loading and other seasonal effects parametrically on annual and semiannual timescales, and we use global soil moisture data sets to correct for displacements excited by hydrological loads on multi-year timescales. We assess the spatial extent and spatial coherence of transient deformation from cross-correlations of the observed GPS time series after correction for the mass loading model. We use dislocation modeling to examine the implied slip, and assess whether such models provide insight into depth and size of the deformation source. Finally, we evaluate alternative hypotheses on Basin and Range rheology in the context of new EarthScope-derived observations of physical state of the Basin and Range lithosphere.

## 2. Data

We use two observational data sets: 1) GPS time series of positions at twenty-two sites in the northern Basin and Range (Figure 1); and 2) Global monthly hydrologic data from land surface models. The second data set is used to model elastic response to surface hydrologic mass loading, and correct for these effects at GPS sites prior to modeling tectonic transients.

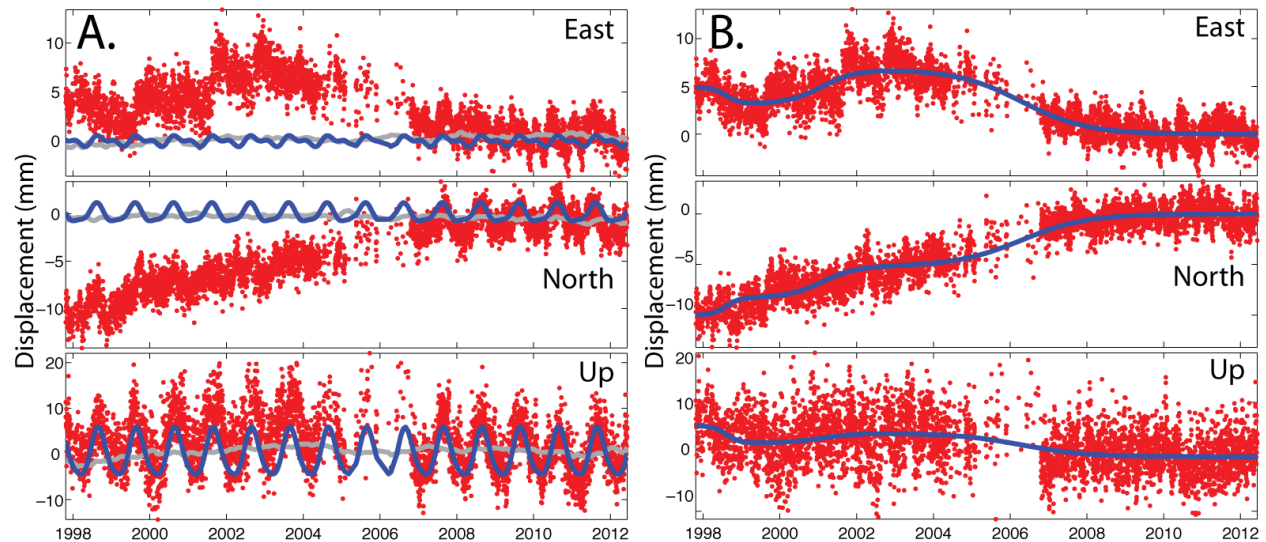


**Figure 2:** Example of GPS time series modeling at site MINE, with final model velocity terms removed. (a) Raw time series (red circles, after correction for hardware changes at 2001.6 and 2006.8). Blue line depicts the half- and one-year period sinusoids estimated from the data; the grey line shows the interannual contribution modeled from GLDAS hydrologic fields. (b) Time series after correction for elastic loading. Blue line represents the best-fitting model of transient deformation from hyperbolic tangent function analysis.

### 2.1 GPS Data

The raw position data used in our analysis are cleaned and unfiltered Scripps Orbit and Permanent Array Center (SOPAC) MEaSUREs combination GPS time series [Bock and Webb, 2012], sampled at daily intervals from July 1996 to June 2012. We corrected the data for offsets associated with antenna and instrument changes catalogued in the site metadata, using a parametric (hyperbolic tangent function) modeling approach detailed in section 3.1. Displacements of the antenna phase center location were estimated using only the hyperbolic tangent and sinusoidal parametric terms. An example raw time series (after correction for

hardware changes and removal of the velocity term) is depicted for site MINE (near Carlin, Nevada) in Figure 2a.

## 2.2 Hydrologic Data

Terrestrial water storage is estimated by merging monthly averages of three hydrologic data fields of the National Oceanic and Atmospheric Administration (NOAA)'s GLDAS (Global Land Data Assimilation System) L4 model [Rodell *et al.*, 2004]. Prior to March, 2000, water storage is re-sampled using a linear surface interpolation from  $1^\circ \times 1^\circ$  spatial resolution to  $0.25^\circ \times 0.25^\circ$  sampling, for consistency with the  $0.25^\circ \times 0.25^\circ$  resolution of the L4 monthly model available from March, 2000 onward. Our terrestrial water storage model sums all four layers of soil moisture in the L4 model (0–0.1, 0.1–0.4, 0.4–1.0, and 1.0–2.0 m), along with the snow water equivalent and total canopy water storage fields, to arrive at a global estimate of total hydrologic mass load in mm of water equivalent thickness (i.e.,  $\text{kg m}^{-2}$  of surface mass load). The GLDAS land surface fields are derived from a combination of several independent climate- and weather-driven land surface models. The model assimilates direct observational data including global satellite measurements of surface temperature, precipitation, soil moisture and snow cover, and it also incorporates operational weather forecasts that, in turn, assimilate surface and sonde measurements relevant to land-surface water flux. The average peak-to-peak annual water storage from the model is contoured within the Basin and Range region in Figure 1 and exhibits, for example, the strong influence of orographic precipitation expected of these mass fields.

## 3. Transient Identification and Modeling

GPS time series are modeled as transient signals of tectonic origin combined with seasonal and annual terms associated with loading, reference frame and other signals, plus interannual variations due to hydrologic loading. Accurate modeling of hydrologic loading response is crucial, particularly when the desired (tectonic) transient deformation signals are of low amplitude, to avoid misidentification of loading effects as tectonic transients. Transients in the Basin and Range have displacements one to two orders of magnitude smaller than those commonly observed in subduction zones, and they are active for much longer periods.

The data analysis performed here can be summarized as a sequence of several steps:

1. GPS time series are preprocessed to remove outliers and correct for offsets of the instrument antenna phase center associated with hardware changes (§2.1).
2. Monthly-sampled global hydrological mass estimates are prepared for the July 1996 to June 2012 epochs of GPS time series examined here, using NOAA's GLDAS L4 land surface model (§2.2).
3. Elastic displacement response to the global hydrologic model is calculated at each GPS site. The resulting three-component displacement time series are interpolated to daily sampling, and amplitudes of best-fitting sine and cosine functions are estimated for periods of six months and one year (Figure 3a). These sinusoids are subtracted from the load-displacement model to isolate the interannual response to hydrologic loading, denoted as  $\bar{x}_{GLDAS}^{ia}(t)$  (Figure 3b).
4. Preliminary timing parameters of a hyperbolic tangent function approximation to tectonic deformation are identified via a combined grid- and gradient-search. Parameters that minimize misfit to the GPS time series are examined further. Timing parameters that are

similar at neighboring sites and do not overlap with other transient events are identified as potential candidates for tectonic modeling.

5. Finally, timing parameters identified as candidates for analysis are held fixed while we invert the GPS observations for total transient displacement, scaling of the interannual load displacement and amplitudes of GPS displacement at seasonal periods.

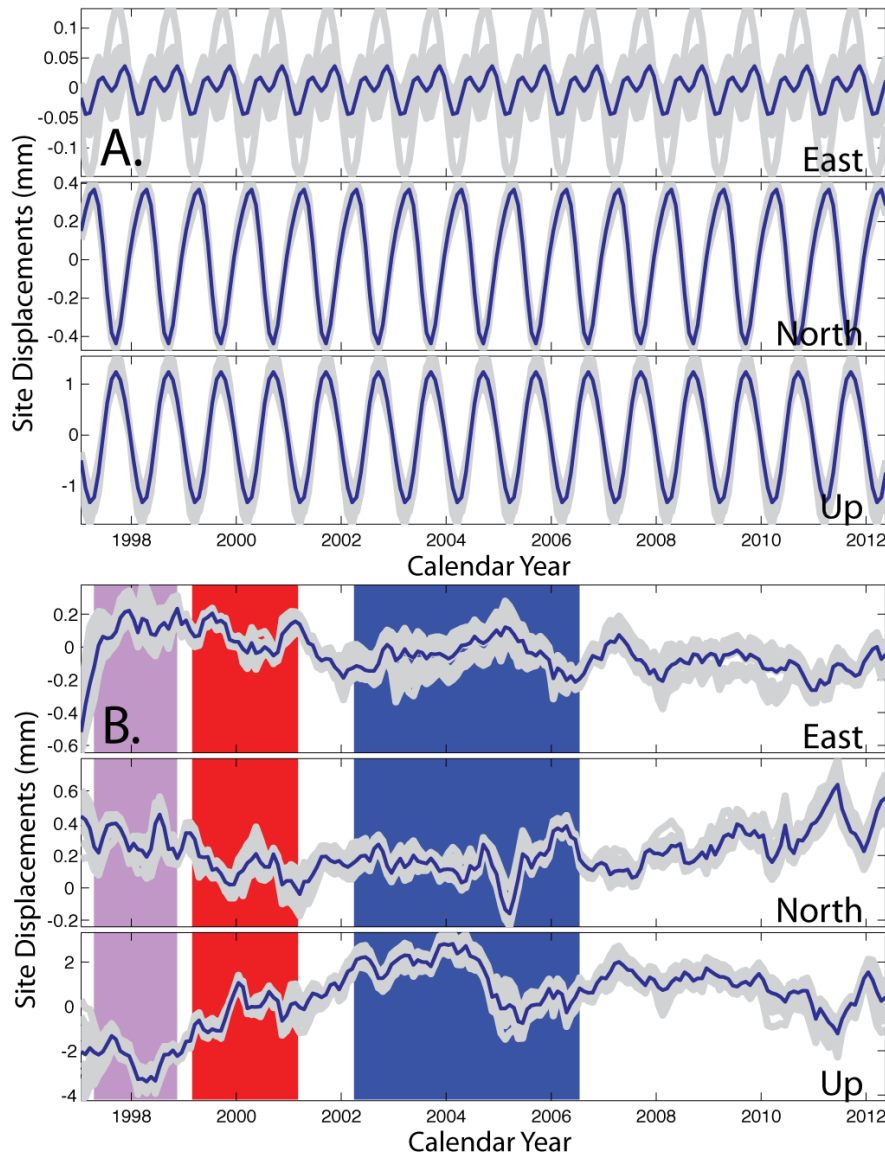


**Figure 3.** Envelope (grey lines) and mean (blue lines) of elastic Earth displacements modeled at the GPS site locations using the GLDAS L4 land surface hydrology model. (a) Six-month plus one-year period sinusoids are subtracted from the model time series and not used; (b) The interannual component (i.e.,  $\bar{x}_{GLDAS}^{ia}(t)$ , with six-month and one-year components removed). Colored bands indicate the approximate timing of the  $\sim 1998.3$  (violet),  $\sim 2000.4$  (red; east-northeastward), and  $\sim 2004.4$  (blue; northwestward) transients.

In the following sections, we describe the estimation of seasonal and hydrologic loading displacement and approach to hyperbolic tangent function analysis (steps 3–5) in greater detail.

### 3.1 Modeling Earth's Elastic Response to Hydrologic Loading

We model hydrologic loading displacements as an elastic Earth response to global climatological models of continental water storage, described in §2.2, in combination with conventional parameterization of sinusoids at periods of six months and one year. The annual and semiannual terms remove hydrologic as well as reference frame effects and other undesired nontectonic signals [e.g., *Dong et al.*, 2002]. Modeling of the elastic response to hydrologic loading assumes a spherical, radially symmetric Earth with Preliminary Reference Earth Model (PREM) [*Dziewonski and Anderson*, 1981] elastic and density properties. Elastic Earth deformation is calculated from spherical harmonic relationships to load Love numbers, as described by *Wahr* [1983]. Model outputs were validated by comparison to Green's function predictions of vertical and horizontal response of PREM to disk loads as described by *Farrell* [1972] (Figure 4). Time series of displacement forced by the GLDAS L4 monthly mass fields are calculated at each GPS site location, and the monthly elastic responses are then interpolated to daily sampling.

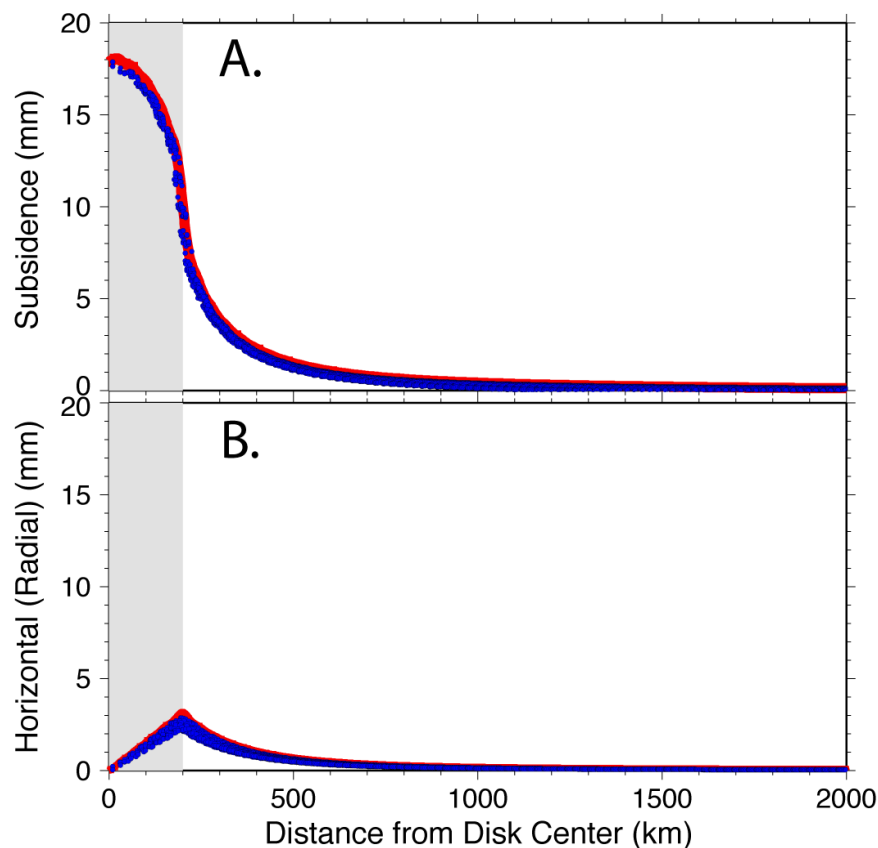


**Figure 4.** Comparison of Green's function [*Farrell*, 1972] (red line) and discretized ( $0.25 \times 0.25^\circ$  mesh; blue dots) models of surface displacements predicted for a 200-km radius disk-load of 1 m water-equivalent thickness (i.e.,  $1000 \text{ kg/m}^2$ ) on a PREM spherical Earth [*Dziewonski and Anderson*, 1981]. Minor differences relate to differences in maximum spherical harmonic degree used ( $l_{max} = 1000$  for the Green's function calculation;  $l_{max} = 720$  for the discrete model) and numerical error in discrete representation of the disk load and its mass derivative. (a) Vertical response (positive downward). (b) Radial horizontal response (positive toward the center of the disk).

We examined two different approaches to representing the surface mass load response. Initially we used only the PREM response to NOAA GLDAS L4 model to represent seasonal and annual load displacements (Figure 3a), as well as interannual and other timescales (Figure 3b). However we found that “corrected” time series after subtraction of these model displacements from observed GPS time series had large residual amplitudes at seasonal/annual periods, particularly in the horizontal components. Poor correspondence between modeled and observed seasonal displacements is not surprising because a large fraction of seasonal variation in GPS displacements arises from other sources, including atmospheric and ocean loading as well as pole tide and other reference frame effects [*Dong et al.*, 2002]. Also, whereas vertical displacements

are sensitive to the regionally-averaged surface mass load, the horizontal displacements are most sensitive to the local derivative of the mass field (e.g., the disk load example in Figure 4). The GLDAS L4 mass model neglects the loading effect of changing water heights in reservoirs, lakes and rivers (including those represented by grey lines in Figure 1), and its 0.25° sampling aliases the ~35-km wavelengths of northern Basin and Range topography, so the scaling of modeled horizontal loading displacements may differ from observations (although the time-dependence should be roughly correct).

To partially overcome ambiguities in the causes of seasonal variation and limitations of the GLDAS hydrologic model, we adopt a hybrid approach that retains (but rescales) the interannual variation of the GLDAS model (Figure 3b), and substitutes a parametric model at seasonal timescales. We invert for amplitudes of sine and cosine terms that best-fit the GLDAS-derived displacement model at periods of 0.5 and 1 year, subtract those from the elastic load displacement model, and substitute sine and cosine amplitudes that best-fit the observed GPS time series at those periods. Thus, the time-dependent description of nontectonic displacement,  $\bar{x}_l$ , incorporates five terms in each of its three components:

$$\bar{x}_l(t) = \bar{a}_0 \circ \bar{x}_{GLDAS}^{ia}(t) + \bar{a}_1 \cos(4\pi t) + \bar{a}_2 \sin(4\pi t) + \bar{a}_3 \cos(2\pi t) + \bar{a}_4 \sin(2\pi t), \quad (1)$$

where  $\circ$  denotes element-wise multiplication;  $\bar{a}_0$  is a three-component constant scale-factor;  $\bar{x}_{GLDAS}^{ia}(t)$  is the interannual component of PREM elastic displacement response to the GLDAS L4 climatological model (Figure 3b);  $\bar{a}_1$  and  $\bar{a}_2$  are amplitudes of sinusoidal displacements at half-year periods; and  $\bar{a}_3$  and  $\bar{a}_4$  are amplitudes of sinusoidal displacements at one-year periods. In practice, we use the GPS observations to invert linearly for the constant parameters  $\bar{a}_0$ ,  $\bar{a}_1$ ,  $\bar{a}_2$ ,  $\bar{a}_3$  and  $\bar{a}_4$  simultaneously with linear inversion for constant parameters in the tectonic model (next section).

### 3.2 Hyperbolic Tangent Function Analysis (HTFA)

Transient displacements associated with slow fault slip can be estimated using hyperbolic tangent function analysis (HTFA) [Larson *et al.*, 2004; Brudzinski *et al.*, 2007]. Anomalous displacements during slow slip events are estimated by fitting the GPS coordinate time series with a function of the form:

$$\bar{x}(t) = \bar{x}_0 + \bar{V}t + \sum_{i=1}^n \frac{\bar{U}_i}{2} \left[ \tanh\left(\frac{t-T_{0i}}{\tau_i}\right) - 1 \right] + \bar{x}_l(t) \quad (2)$$

in which  $\bar{x}(t)$  are three-component GPS site coordinates at time  $t$ ,  $\bar{x}_0$  are coordinates at a reference time,  $\bar{V}$  is a background or “steady-state” velocity,  $\bar{U}_i$  is anomalous displacement during the  $i^{\text{th}}$  of  $n$  slow slip events,  $T_{0i}$  is the median time of the  $i^{\text{th}}$  event,  $\tau_i$  scales the period over which the event occurred and  $\bar{x}_l$  is displacement due to nontectonic phenomena as described in the previous sub-section.

If  $T_0$  and  $\tau$  are specified, all of the remaining unknown constants in equations (1) and (2) can be estimated from linear least-squares inversion. We begin by assuming just one transient event occurred and use a grid search algorithm over  $T_0$  and gradient search over  $\tau$  to identify weighted root-mean-square (wRMS) misfit minima that may correspond to deformation transients. Linear parameters of velocity and transient displacement in all three components of the GPS time series are estimated for each  $(T_0, \tau)$  parameter pair via least squares minimization, weighted by the formal inverse variance of GPS coordinate estimates. Estimates of  $(T_0, \tau)$  that minimize

weighted-RMS misfit in time series of misfit versus  $T_0$  (Figure 5) then are examined further to determine whether they are promising candidates for analysis as transient deformation events.

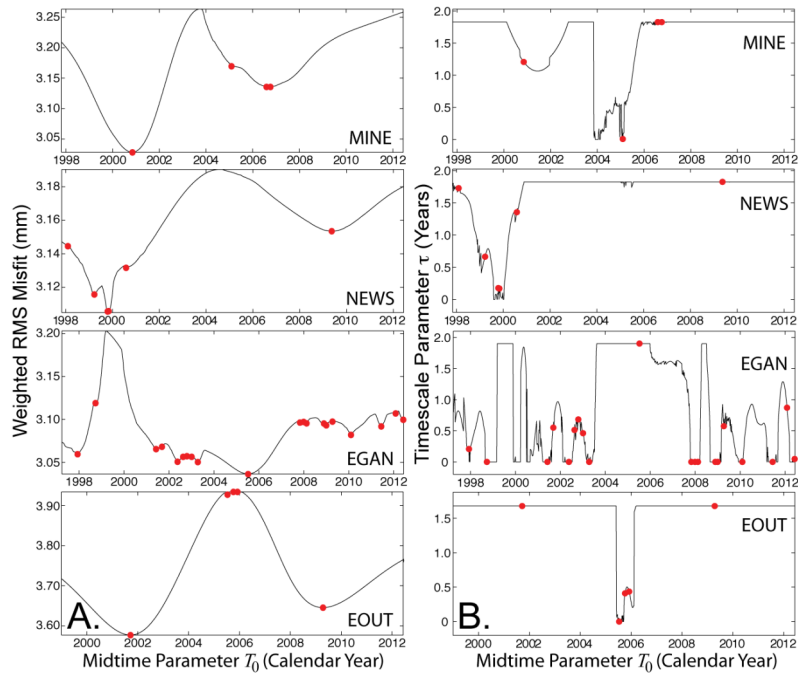


**Figure 5.** Automated search results for timing parameters of possible transient deformation assuming a single event. (a) Time series of RMS misfit to measured displacement for several sites, as a function of assumed  $T_0$ .  $T_0$  parameters that do not yield misfit minima at approximately the same time at several neighboring sites can be rejected as candidates for tectonic transient events. (b) Best-fitting timescale parameters  $\tau$  as a function of  $T_0$ ; 90% of the transient displacement occurs over a period of roughly  $3.8\tau$ . Brief ( $\tau < 0.5$  year) events associated with extremely localized minima are generally ignored, and very long timescale parameters that result in overlapping transient events are either rejected as candidate events or shortened in final, multi-event analysis.

Several additional criteria must be met before further analyzing a displacement anomaly. First, HTFA modeling must minimize misfit at several different sites at approximately the same (independently determined) midtime  $T_0$ , and with similar timescale  $\tau$  (Figure 5). Second, total displacement at a majority of these sites must significantly exceed the 95% confidence interval of the displacement estimate. Finally, abrupt transient displacements ( $\tau$  less than about 0.5 year) are ignored, as earlier studies of Basin and Range slow fault slip involved timescales of order a year or longer.  $T_0$  and  $\tau$  parameters estimated by grid and gradient search assuming only one event are further refined manually to ensure that multiple transients do not overlap. These criteria greatly reduce the likelihood of false positives. As a final step, linear parameters are estimated combining all of the  $T_0$  and  $\tau$  parameters identified at each site, and the nonlinear timing parameters are re-estimated iteratively for each event to optimize the fit. Often the final estimates of best-fitting timescale parameter  $\tau$  are very different for the final (multi-event) models than those which minimized misfit in the preliminary (single-event) models shown in Figure 5. Once the best-fitting multi-event model has been finalized, formal parameter uncertainties of velocity and displacement are scaled using the weighted-RMS misfit to yield a reduced  $\chi^2$  parameter of one.

In the example time series shown in Figure 2, subtraction of the loading model reduces weighted RMS misfit from 3.2 mm for the raw time series to 2.5 mm. Using likelihood statistics for the  $F$ -cumulative distribution, the improvement is significant at  $> 5\sigma$  confidence even when one accounts for the larger number of parameters (increased from six for a line-fit to twenty-one for line-fit plus load scaling and seasonal model amplitudes). The high confidence is a consequence of the large number of daily observations in three components of a  $>14$  year time series. Removing the tectonic model further reduces the misfit to 2.3 mm, also a significant

improvement at  $> 5\sigma$  confidence. The combination of loading and tectonic models similarly reduces variance significantly relative to raw time series at all of the other GPS sites examined in this study.

## 4. Results

### 4.1 Load modeling

Peak-to-peak variations in displacement for our models of the interannual component of loading are of order 7 mm in the vertical and 1 mm in each of the horizontal components (Figure 3b). Consequently, removing the interannual elastic load response is critically important for identification of long-timescale, low amplitude transients in low-strain environments such as the Basin and Range. Inclusion of the GLDAS L4 model of interannual hydrologic loading significantly reduced misfits at all GPS sites, particularly in the North and Up components, and subtracting parametric estimates of annual and semiannual terms reduced misfits even further. The scaling terms,  $a_0$ , derived from the analysis are  $0.2\pm 1.2$  in the east component,  $1.2\pm 1.1$  in the north and  $1.1\pm 0.6$  in the vertical over all sites. The approximate unit-scaling of the GLDAS predictions, coupled with the reduction of variance (significant at  $>5\sigma$  confidence), suggest that the method developed here does mitigate long-timescale effects of elastic Earth deformation response to hydrologic mass.

### 4.2 Transient modeling

Previous analyses [Davis *et al.*, 2006; Wernicke and Davis, 2010] focused on the east components, which are shown in Figure 6ab after removal of velocity and load-model terms. We identify three transients that affected a majority of the sites, with  $T_0$  around 1998.3 (period  $\sim 1.6$  year), 2000.4 (period  $\sim 2$  years) and 2004.4 (period  $\sim 4.3$  years) (Figure 6c). These differ slightly from the transient events interpreted from geodogram analyses by Wernicke and Davis [2010], which identified transients in the western Basin and Range in  $\sim 2000$ , 2004 and 2006 (with an opposite-directed transient in the eastern Basin and Range also in 2006). In our analysis, the “steady-state” velocity term at almost all sites is defined by approximately linear behavior during the five-year period from 2007 to 2012 (e.g., Figures 2 and 6), which was unsampled in early studies by Davis *et al.* [2006] and Wernicke *et al.* [2008]. Those analyses used motions during the  $\sim 1997$ –2000 epoch as a steady-state reference, a time-frame which our analysis suggests is anomalous (Figures 2 and 6). Separation of “reference” from “transient” motion is inherently ambiguous, but it is reasonable to define the reference velocity based on the longest period of quasi-linear motion.

### 4.3 Cross-correlation analysis

We group the sites into two categories based on similarity of transient behavior (Figure 6a–c). The analysis finds similar transient displacements throughout the whole of the Basin and Range, not just at western sites as interpreted in previous studies [Davis *et al.*, 2005; Wernicke and Davis, 2010]. The similarity we qualitatively infer based on timing and duration of transient events is confirmed by quantitative comparison using cross-correlation of the raw time series with mean, velocity and seasonal/loading models removed (Figure 7a). Cross-correlations of the load-corrected raw time series are strongest in the North component, with correlation coefficients  $r_N = 0.55\pm 0.09$  as compared to  $r_E = 0.50\pm 0.10$  in the East and  $r_U = 0.42\pm 0.11$  vertical. The differences reflect GPS coordinate errors that are generally largest in the vertical and smallest in the North component, in addition to the relative amplitude of coherent signal in each component.

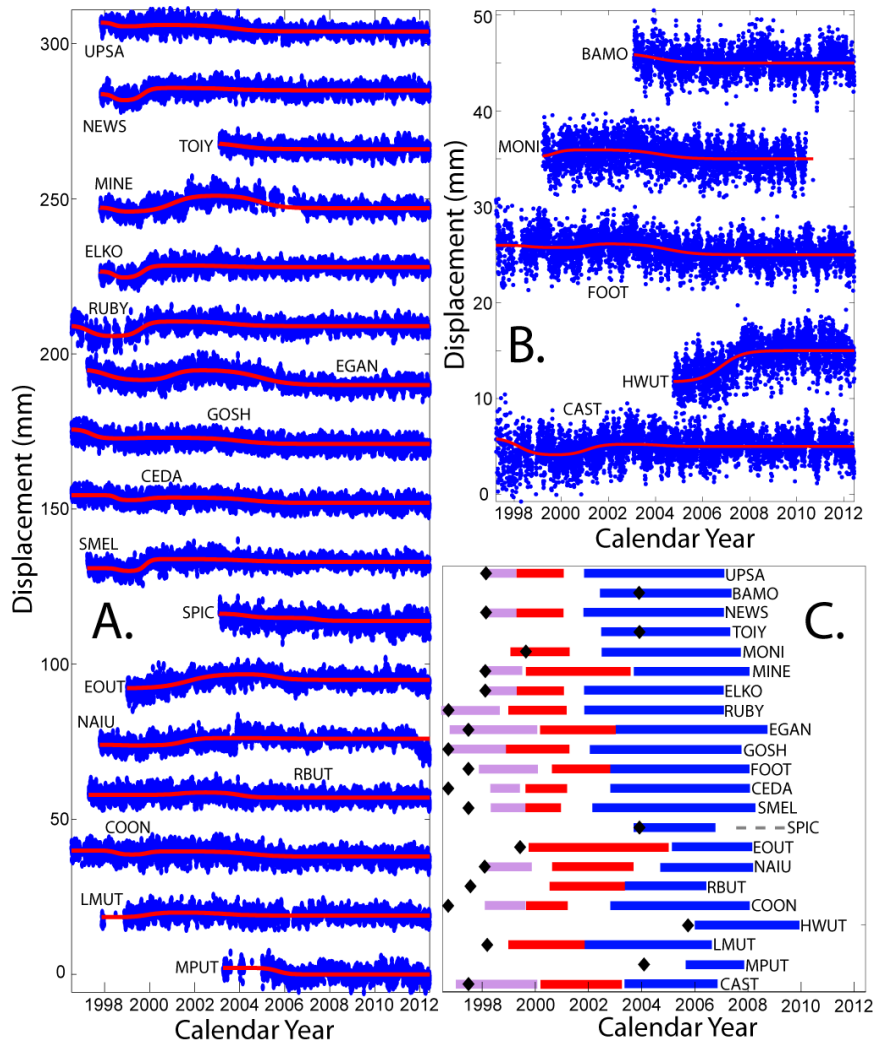


**Figure 6:** East components of site motion (blue circles) and the best-fitting hyperbolic tangent function models (red lines) after removing velocity and elastic loading models. Sites are ordered west (top) to east (bottom). (a) Sites with relatively similar transient behavior. Sites in *Wernicke and Davis’* [2010] western domain (UPSA to EGAN) tend to have larger displacements, but events with similar timing and duration are also identified at many eastern sites. (b) Atypical sites generally are either shorter time series or are located east of the Wasatch fault. (c) Timing and approximate duration of the  $\sim 1998.3$  (violet),  $\sim 2000.4$  (red), and  $\sim 2004.4$  (blue) events at each of the sites. Black diamonds indicate the beginning of each time series.

Figure 7b depicts the correlation coefficients for residual time series after removing the mean, trend, load model and best-fit HTF models of transient tectonics. The correlation coefficients remain uniformly positive and average  $\sim 0.5$ . One significant contributor to large positive correlations in both Figure 7a and 7b is common-mode error: We purposely chose to use GPS time series that were not spatially filtered [e.g., *Wdowinski et al.*, 1997] because filtering to remove common-mode errors may inadvertently remove part of the widespread tectonic transient signal we are examining here. Consequently, identical errors in satellite orbit estimates and daily reference frame realization are present in all of the sites. However, these types of errors will be identical in poorly-correlated as well as strongly-correlated site pairs. A second contributor is likely to be errors in modeling of the elastic loading displacement and other nontectonic signals at each site, arising from loading effects at sub-monthly timescales, errors in the GLDAS L4 climatological model, unmodeled water storage in reservoirs, lakes and rivers, and other coherent nontectonic signals in the time series. Figures 7a and 7b exhibit a block structure (highlighted by dashed black lines) indicating that residual error is more similar at western sites than other sites. For example, in Figure 7b, correlation coefficients in the “western” block of sites from UPSA to SMEL are  $r_E = 0.58 \pm 0.06$ ;  $r_N = 0.64 \pm 0.04$ ;  $r_U = 0.51 \pm 0.07$ , while in the remaining eastern block of sites they are lower with  $r_E = 0.44 \pm 0.07$ ;  $r_N = 0.46 \pm 0.06$ ;  $r_U = 0.35 \pm 0.09$ . Cross-correlations of eastern to western sites are intermediate to those within the two blocks ( $r_E = 0.50 \pm 0.07$ ;  $r_N =$

$0.53 \pm 0.06$ ;  $r_U = 0.40 \pm 0.09$ ), which indicates that residual motions at the eastern sites generally reflect larger contributions from truly spatially-incoherent processes, but nevertheless include similar coherent motions to those at western sites. Residuals at eastern sites near the densely-populated Wasatch front likely include (for example) anthropogenic effects associated with groundwater storage and withdrawal. The inference that these sites are inherently “noisier” is reinforced by larger weighted RMS misfits of HTFA models of the eastern sites relative to western sites ( $2.6 \pm 0.4$  versus  $2.2 \pm 0.1$  mm, respectively).

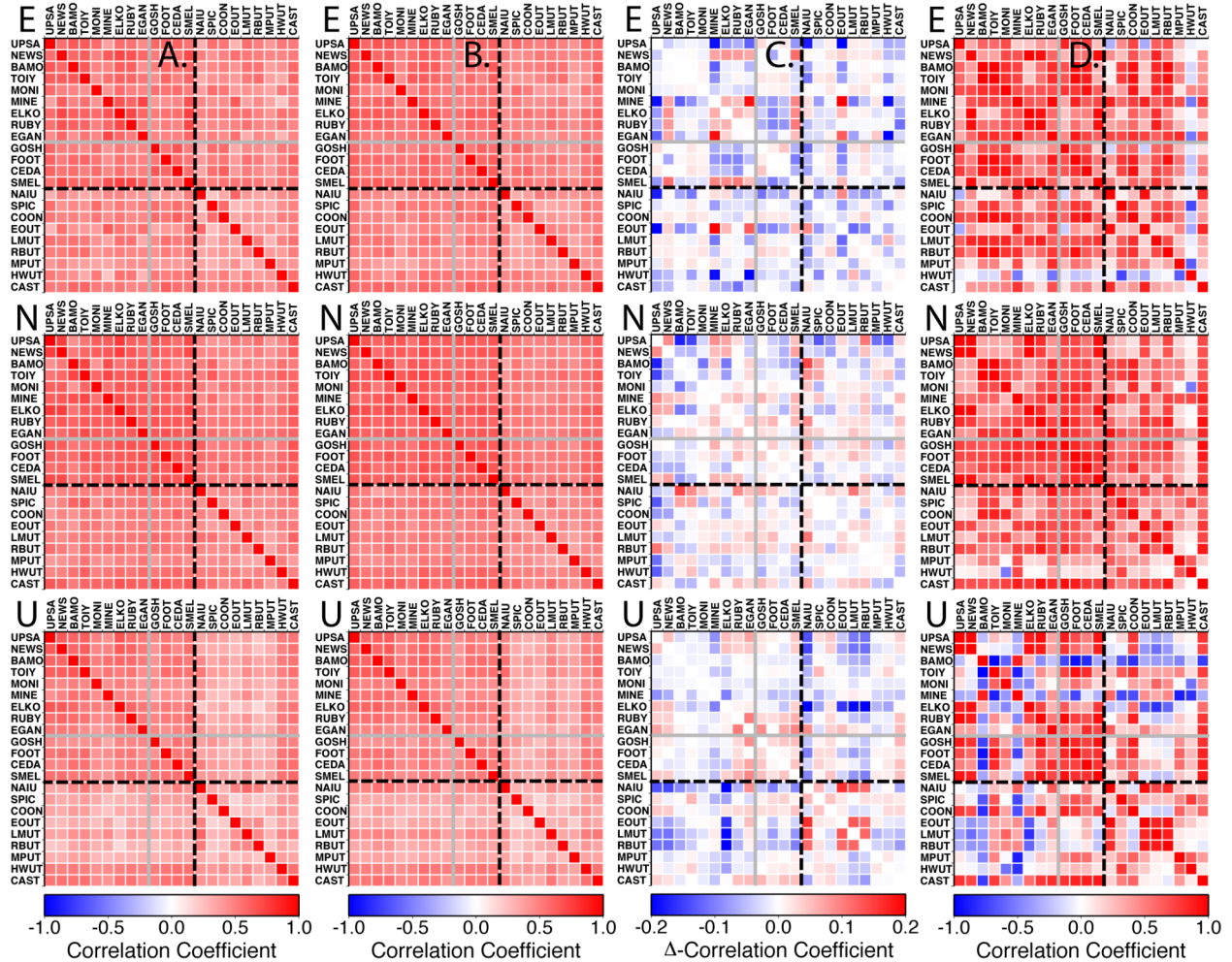


**Figure 7.** Cross-correlation matrices quantifying the similarity of pairs of GPS time series, in the East (E), North (N) and Up (U) components. Sites are ordered from west to east going top to bottom and left to right. Grey lines delineate the correlation matrix “block structure” expected for the western and eastern domains distinguished in *Wernicke and Davis* [2010]; dashed black lines delimit the block structure suggested by this analysis. (a) Cross-correlation coefficients of raw measured time series with mean, velocity and elastic loading model removed. (b) Cross-correlation coefficients of measured time series with loading model and tectonic (HTFA) model removed. (c) Change in coefficients before and after subtraction of the tectonic model (i.e., Figure 7a minus 7b). (d) Cross-correlations of the HTFA models of “tectonic” transient motion.

The changes in cross-correlation coefficients with versus without the HTF models of tectonic transient deformation are generally small (Figure 7c) and have variable sign. This is partly because the modeled component of transient deformation is not the dominant source of positive

correlation in Figure 7a, and partly because the HTF models themselves have both positive and negative time correlation (Figure 7d). The variability of changes in Figure 7c is strongly related to cross-correlation coefficients of the model time series, shown in Figure 7d: If one compares the off-diagonal terms in the two figures, the correlation coefficient is 0.55, which is significant at very high confidence. However, changes depicted in Figure 7c also reflect relative sizes and sign of interference between the HTF model and whatever signals dominate the high cross-correlation coefficients between GPS sites depicted in Figures 7ab.

#### 4.4 Transient displacements

The transient event identified in the earliest part of the time series, around 1998.3, begins before or coincident with the start of GPS observations at most sites (Figure 6c). Consequently the ~1998 displacements are effectively unconstrained, and we do not attempt to estimate those displacements or model them here. Anomalous displacements during the ~2000.4 event are generally eastward and northward, as listed in Table 1 and depicted in Figure 8a. Displacements during the ~2004.4 event are westward and northward (Table 2 and Figure 9a). Horizontal displacements of the tectonic transients exceed the range of variation in the load model by a factor of two to ten at most sites.

**Table 1:** Displacements and uncertainty estimates during the 2000.4 transient of period ~ 2 years by HTFA analysis of the GPS coordinate time series.

Site	Displacement (mm)			One-Sigma Uncertainty (mm)		
	East	North	Up	East	North	Up
UPSA	0.5	2.9	-6.4	0.2	0.2	0.2
NEWS	4.1	2.8	-5.5	0.2	0.2	0.2
MONI	0.8	-0.1	0.2	0.2	0.3	0.3
MINE	5.3	2.2	2.7	0.2	0.2	0.3
ELKO	3.9	2.1	-6.6	0.2	0.2	0.3
RUBY	4.8	0.7	-5.8	0.2	0.3	0.3
EGAN	3.3	0.6	2.8	0.1	0.2	0.3
GOSH	0.3	0.9	-4.1	0.1	0.2	0.3
FOOT	0.4	0.4	-1.1	0.1	0.2	0.2
CEDA	0.8	0.0	0.8	0.1	0.2	0.2
SMEL	3.9	1.7	-3.1	0.1	0.2	0.2
EOUT	4.6	1.9	14.5	0.2	0.3	0.4
NAIU	2.4	1.3	10.6	0.1	0.2	0.2
RBUT	0.8	1.4	8.4	0.1	0.2	0.3
COON	1.1	-0.6	-4.7	0.2	0.4	0.4
LMUT	1.5	-1.1	6.6	0.2	0.3	0.3
CAST	1.2	0.9	-0.7	0.1	0.2	0.2

*Wernicke and Davis* [2010] previously identified the ~2000.4 event as an eastward and northward velocity anomaly, referred to as a “slowing” of Basin and Range extension (although the north component represents an acceleration of northward steady-state motion in the western Basin and Range). Our ~2004.4 event overlaps an eastward subevent that *Wernicke and Davis* [2010] interpreted to have occurred late 2003, but the direction is westward and thus more consistent with a velocity anomaly they observed ~2006 (which our 2004.4 event also overlaps). Arguably the most important difference between our analysis and that of *Wernicke and Davis* [2010] is the recognition here that smaller, but significant, displacements occurred during these epochs in the eastern Basin and Range at roughly the same time and in the same direction as transient motions in the western Basin and Range.

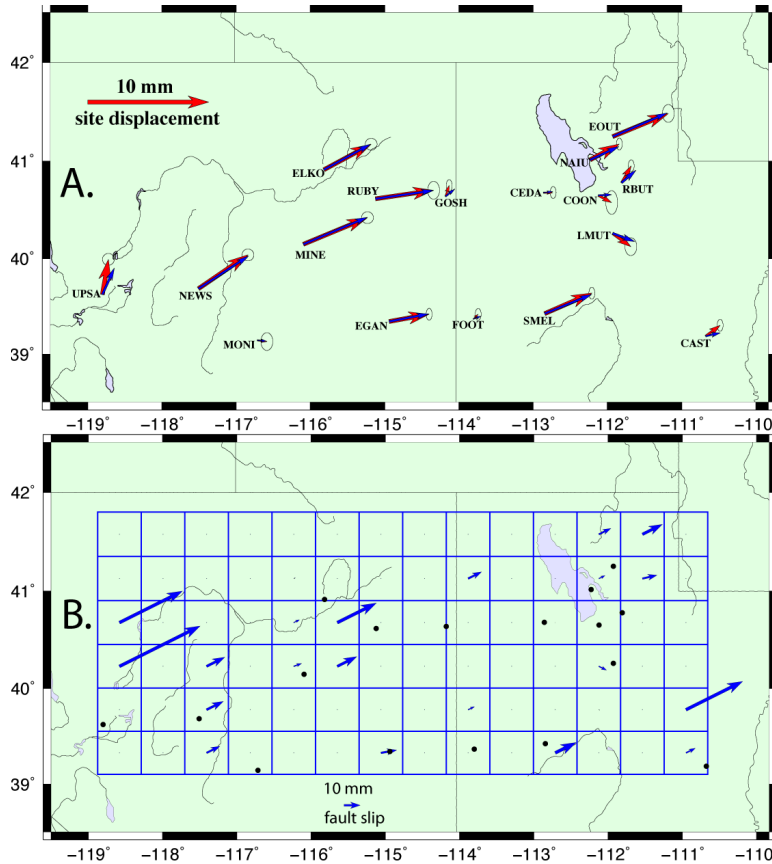


**Figure 8.** Slip modeling of  $\sim 2000.4$  transient displacements. (a) Measured (red vectors, with  $1\sigma$  confidence ellipses) and modeled (blue vectors) horizontal displacements. (b) Distribution of slip on  $50 \times 50$  km horizontal dislocations at 15 km depth, with a minimum-moment constraint. The moment release is equivalent  $M_w$  6.9.

## 5. Slip Modeling

We model displacements of the transients at  $T_0 \sim 2000.4$  and  $2004.4$  on detachment-like horizontal dislocations (i.e., zero-degree dip) at 15 and 30 km, reflecting the possible range of depths for frictional slip near the bottom of the seismogenic zone. When dislocation dip, depth, length and width are specified, strike-slip (north-south;  $S_0^{ss}$ ) and dip-slip (east-west;  $S_0^{ds}$ )

components of total slip relate linearly to measured surface deformation. We discretize a hypothetical horizontal surface as  $50 \times 50$  km patches with uniform slip on each patch. The inversion scheme uses quadratic programming with inequality constraints that include eastward dip-slip greater than zero for  $\sim 2000.4$  displacements and less than zero for  $\sim 2004.4$ ;  $-S_0^{ds} \leq S_0^{ss} \leq S_0^{ds}$ ; a maximum slip of 10 cm, and a damping constraint to minimize the total moment release of slip.

We inverted models using all three components of transient displacement in the data vector as well as models using only the horizontal components. Estimates of transient vertical displacements have generally low signal-to-noise ratio however, particularly in the eastern Basin and Range where many sites exhibit ratios of vertical-to-horizontal displacement that are improbably high for low-angle normal fault slip and have no discernible pattern (and hence are probably perturbed by unmodeled deformation effects of lake-loading, groundwater withdrawal and perhaps soil expansion effects). Consequently we present results only for modeling of the horizontal displacements here. The modeled displacements and estimated slip distributions for the two transients at 2000.4 and 2004.4 are shown in Figures 8 and 9 respectively for the dislocation models at 15 km depth. The equivalent moment magnitudes are  $M_w = 6.9$  and  $7.0$  for the  $\sim 2000.4$  and  $\sim 2004.4$  events, respectively.  $M_w = 6.9$  is near the bottom of the 6.8–7.2 range estimated by *Wernicke et al.* [2008] for their circa-2000 event, consistent with the minimum-moment constraint.

**Table 2:** Displacements and uncertainty estimates during the 2004.4 transient of period ~ 4.3 years by HTFA analysis of the GPS coordinate time series.

Site	Displacement (mm)			One-Sigma Uncertainty (mm)		
	East	North	Up	East	North	Up
UPSA	-2.1	2.3	1.3	0.1	0.2	0.2
NEWS	-0.8	2.0	-0.4	0.2	0.2	0.2
BAMO	-1.0	4.8	-2.8	0.2	0.3	0.3
TOIY	-2.1	1.5	1.7	0.2	0.3	0.3
MONI	-1.0	0.7	0.5	0.2	0.3	0.3
MINE	-4.2	3.7	-3.8	0.2	0.3	0.2
ELKO	-0.5	1.7	-3.3	0.1	0.2	0.2
RUBY	-1.5	1.8	1.9	0.1	0.2	0.2
EGAN	-4.9	2.2	0.3	0.2	0.2	0.2
GOSH	-2.0	2.4	2.4	0.2	0.2	0.2
FOOT	-1.2	1.9	3.4	0.2	0.2	0.2
CEDA	-1.7	0.7	3.4	0.1	0.2	0.2
SMEL	-0.9	1.8	1.7	0.1	0.2	0.2
SPIC	-1.4	2.1	4.8	0.2	0.3	0.3
HWUT	3.3	1.5	4.9	0.2	0.3	0.5
EOUT	-1.9	0.8	5.0	0.2	0.3	0.3
NAIU	-0.2	2.3	2.7	0.1	0.2	0.2
MPUT	-2.1	1.3	7.2	0.3	0.4	0.4
RBUT	-1.7	1.3	5.4	0.2	0.2	0.2
COON	-1.7	1.0	3.1	0.2	0.3	0.3
LMUT	-1.0	1.9	7.7	0.2	0.3	0.2
CAST	-0.3	2.2	2.1	0.1	0.2	0.2

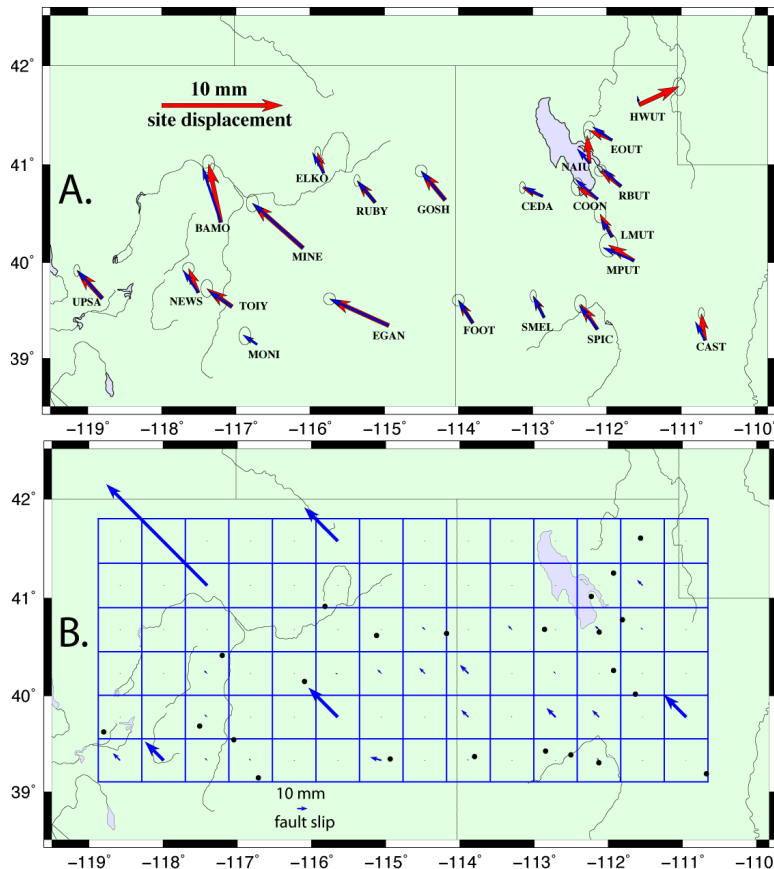


**Figure 9.** Slip modeling of ~2004.4 transient displacements. (a) Measured (red vectors, with  $1\sigma$  confidence ellipses) and modeled (blue vectors) horizontal displacements. (b) Distribution of slip on  $50 \times 50$  km horizontal dislocations at 15 km depth, with a minimum-moment constraint. The moment release is equivalent  $M_w$  7.0.

The models of dislocations at 30 km depth (i.e., a detachment at the Moho) are not shown, but they have similar misfits, similar directions, and similar spatial distributions of slip (albeit with magnitudes of the slip vectors that differ by typically 10–50%). Consequently, modeling of the GPS data alone cannot distinguish the likely depth of deformation source for Basin and Range transients.

Inverted slip in Figures 8-9 is highly underdetermined by sparse sampling at the GPS sites, and hence nonunique. A different set of inequality and regularization constraints would produce very different models. The two robust (hence useful) conclusions to be drawn from these modeling exercises are (1) the available data are equally well-fit by slip on shallow or deep detachment faults, and (2) the strain moment released during these events has minimum equivalent magnitudes  $M_w \sim 7$ .

## 6. Discussion

### 6.1 Implications for elastic load deformation

Transient tectonic deformation in the northern Basin and Range is small (of order half a cm at most sites) and takes place over timescales of several years, so separating it from other signals and noise fields is challenging at best. Estimation and removal of elastic loading effects is critically important in this context. *Davis et al.* [2006] examined the elastic loading effects of water-levels in the Great Salt Lake and atmospheric pressure variations, but did not explicitly remove mass loading deformation from the time series. *Wernicke et al.* [2008] and *Wernicke and Davis* [2010] used a Kalman-filtering approach that removes signals at annual and semiannual periods, but with stochastically varying amplitudes [*Bennett*, 2008]. Our analysis instead used independent climatological data to estimate and remove interannual displacements by hydrologic loading, plus a seasonal correction with constant amplitude. This likely performs less well than the *Bennett* [2008] approach at short periods, but will be more accurate on timescales of two to five years that are most relevant to this analysis. The predicted interannual variations are small relative to our estimates of transient displacements. They vary only slightly across the network at any given time (Figure 3b), indicating that they are dominated by mass variations that are spatially correlated at regional scales.

Visual comparison of the interannual components of the GLDAS-derived hydrologic loading model to the timing and directions of estimated transients (Figure 3b) shows no obvious relationship between the two. However, as noted previously, our analysis neglects loading by rivers, lakes and reservoirs. By far the most significant of these mass loads is the Great Salt Lake [*Elósegui et al.*, 2003], which recorded more than 3 m of lake-level variation during the 1997–2012 observation period over an area roughly equivalent to that of a 40-km radius disk, with maximum in June of 1999 and minimum in October 2010. Horizontal motions associated with the Great Salt Lake would be of order several mm at the nearest sites, in a direction radial from the lake center, and decay with distance (e.g., Figure 4). The relative uniformity of direction of estimated transient motions in the eastern Basin and Range (Figures 8a and 9a) suggests that lake levels are not the dominant deformation source except perhaps at sites such as NAIU and COON that are within a few tens of km of the lakeshore.

Despite neglecting surface water mass fields, the GLDAS data appear to characterize interannual variations in hydrologic mass loading fairly well, as evidence by our model estimates of linear scaling parameters  $a_0 \sim 1$  in the north and up components. Signals aliased by GLDAS  $0.25^\circ$  spatial sampling likely are dominated by groundwater cycles in individual basins. Horizontal displacement response should switch sign depending on where a GPS site is located with respect to the nearest adjacent basin, and this variable sign of the local mass derivative is probably responsible for the smaller mean of scaling coefficients,  $a_0 \sim 0.2 \pm 1.2$ , estimated for the east component of interannual motions.

Amplitudes of the annual and semiannual sinusoids estimated from the GPS data are much less consistent with those predicted by the GLDAS model. GPS-derived annual sinusoids have amplitudes  $0.6\pm 0.3$ ,  $0.7\pm 0.4$  and  $5.2\pm 0.7$  mm in the east, north and up directions respectively; corresponding GLDAS-modeled semiannual amplitudes are  $0.3\pm 0.1$ ,  $0.1\pm 0.1$  and  $1.2\pm 0.4$  mm. The GLDAS predictions of annual and semiannual amplitudes are much less spatially variable (Figure 3a) and a factor of two to five smaller, with combined peak-to-peak amplitudes  $<0.1$ ,  $<0.4$  and  $<1.5$  mm in the east, north and up respectively. The poorer performance of GLDAS fields in predicting subannual relative to interannual GPS displacements may mean that non-hydrologic contributions from atmospheric and ocean loading, pole tide and other reference frame effects, thermal contraction and atmospheric delay mismodeling effects [e.g., Dong *et al.*, 2002] contribute a very significant fraction of the total position power on these timescales. Alternatively, errors in representation of localized spatial variance at short timescales in the GLDAS model may be significantly reduced in longer timescale ensemble averages.

## 6.2 Implications for HTF analysis of tectonic transients

A full accounting of tectonic versus common-mode error contributions to site cross-correlation in Figure 7 is beyond the scope of this analysis, but Figure 7b-d suggests tectonic transient deformation is not the dominant contributor to high cross-correlation of GPS time series unless there is significant transient tectonic deformation that remains unmodeled by the hyperbolic tangent representation adopted here. Earlier analyses of these GPS time series that used smoothing by Kalman filtering and/or velocity analyses [Davis *et al.*, 2006; Wernicke and Davis, 2010] differ from our results in ways that suggest transient deformation on shorter ( $<$  two-year) timescales may be poorly represented by the parametric approach adopted here. The primary advantage of HTFA as described in this study is a small number of parameters, and hence a relatively robust estimate of total displacement during an event that can be used for modeling like that depicted in Figures 8-9. The disadvantage however is that the HTF poorly represents some finer details of the transient behavior.

## 6.3 Summary of new observations regarding Basin and Range transient deformation

Our analysis of Basin and Range GPS displacements reveals two new observations that may help to illuminate the deformation process. One observation is that motions accelerate uniformly northward during both the  $\sim 2000.4$  and  $\sim 2004.4$  events, despite a switch in sign of the east component of motion during these events (Figures 8-9). A second observation is that the events appear to influence all of the Basin and Range, as opposed to just one side or the other. These observations are reinforced by strong cross-correlation of the horizontal components in all of the model time series ( $r_E = 0.49\pm 0.34$ ;  $r_N = 0.57\pm 0.25$ ;  $r_U = 0.22\pm 0.49$  in Figure 7d). There is also strong similarity of the block structure in the model time series as depicted in Figure 7d with that of the load-corrected measurements in Figure 7a (e.g.,  $r_E = 0.63\pm 0.23$ ;  $r_N = 0.68\pm 0.19$  for the western block of model time series versus  $r_E = 0.30\pm 0.40$ ;  $r_N = 0.48\pm 0.25$  for the western block), reinforcing the interpretation that transient tectonic behavior (modeled and unmodeled) is at least partly responsible for the overall correlation of GPS time series.

## 6.4 Implications for tectonic deformation mechanism

The observations described in §6.3 significantly constrain the mechanism for Basin and Range transient deformation. The northward motions observed during both the (eastward)  $\sim 2000$  and (westward)  $\sim 2004.4$  events argues against simple slowing or acceleration of tectonically-driven extensional slip on a megadetachment surface (despite the fact that our slip modeling depicted in

Figures 8-9 essentially assumes that is the case). Implied decoupling of the direction of dislocation during transient events from the direction of long-term tectonic forcing suggests either that the deformation mechanism is extremely sensitive to small perturbations in the stress field, or that localized perturbations can propagate over very large distances. Lack of apparent temporal correlation of transient events with stress forcing by the hydrologic cycle, which is by far the largest known contributor to stress variations on relevant temporal and spatial scales, further indicates that the deformation mechanism must have some sort of state-dependence: that is, there must be some rheological mechanism to introduce strong temporal nonlinearity in the relationship of stress to strain.

### **6.5 Rheological evaluation of proposed frictional detachment at Moho depth**

Previous analyses interpreted the ~2000.4 event as an acceleration of west-domain detachment slip, resulting in block-like eastward translation of the “hanging-wall” [Davis *et al.*, 2006; Wernicke *et al.*, 2008] and (unsampled) focusing of extension within the Walker-Lane seismic belt. The ~2004.4 event conversely was interpreted as a brief cessation of slip [Wernicke and Davis, 2010]. Wernicke *et al.* [2008] discuss a mechanism for detachment slip at the Moho that invokes low-temperature crystal plastic (or “semi-brittle”) deformation of olivine. They base this hypothesis on well-reasoned arguments for decoupling of long-term deformation in the upper crust and uppermost mantle, coupled with field observations of rheological behavior in exhumed detachments and xenoliths, related inferences of crustal composition and mantle water content, and lithospheric viscosity structure estimated by Pleistocene lake and postseismic rebound studies.

The Moho detachment hypothesis of Wernicke *et al.* [2008] relies in part on inferences that the crust does not deform significantly via ductile flow, and that the uppermost mantle is within a low-temperature plasticity rheological regime (i.e., near-Moho rocks deform primarily by localized shear dislocation within the transitional spectrum from velocity-strengthening friction to flow). These inferences rely in turn upon two key assumptions regarding the physical state of the lithosphere in the northern Basin and Range vicinity of the GPS network. The first is that low mantle water content measured in xenoliths from a location ~100 km south of the network is representative of the mantle beneath the network. Dixon *et al.* [2004] interpreted higher water content in the Cordilleran mantle from xenoliths found elsewhere, including the Basin and Range, but Wernicke *et al.* [2008] point out that water in the Basin and Range mantle may have been extracted by voluminous mid-Tertiary melt production. A second key assumption holds that the quartz content of the Basin and Range lower crust is negligible. Quartz is very fluid at likely Moho temperatures, and any significant amount of lower crustal flow would serve to decouple upper crustal from mantle deformation, circumventing formation of a detachment at the Moho.

The Moho megadetachment hypothesis pre-dates recent transformational analyses of geophysical data sets collected by the Plate Boundary Observatory (PBO) and USArray components of the EarthScope facility. Studies of USArray data, particularly the relatively high-density (~70 km spaced) Transportable Array seismic data, have shed significant new light on questions regarding composition, temperature and fluids in the western United States. For example, receiver function analyses [Lowry and Pérez-Gussinyé, 2011] indicate that the thickness of the crust under GPS sites within the Basin and Range averages  $31 \pm 3$  km. Also, tomography of the uppermost mantle using the Moho refraction ( $P_n$ ) phase [Buehler and Shearer, 2010] can be used in combination with mineral physics to estimate Moho temperature [Schutt *et al.*, 2013]. Final estimates of  $P_n$

velocity are somewhat sensitive to the assumed starting model, but if one conservatively adopts models that yield the lowest temperature estimates, the Moho averages  $775 \pm 40^\circ\text{C}$  in the study region.

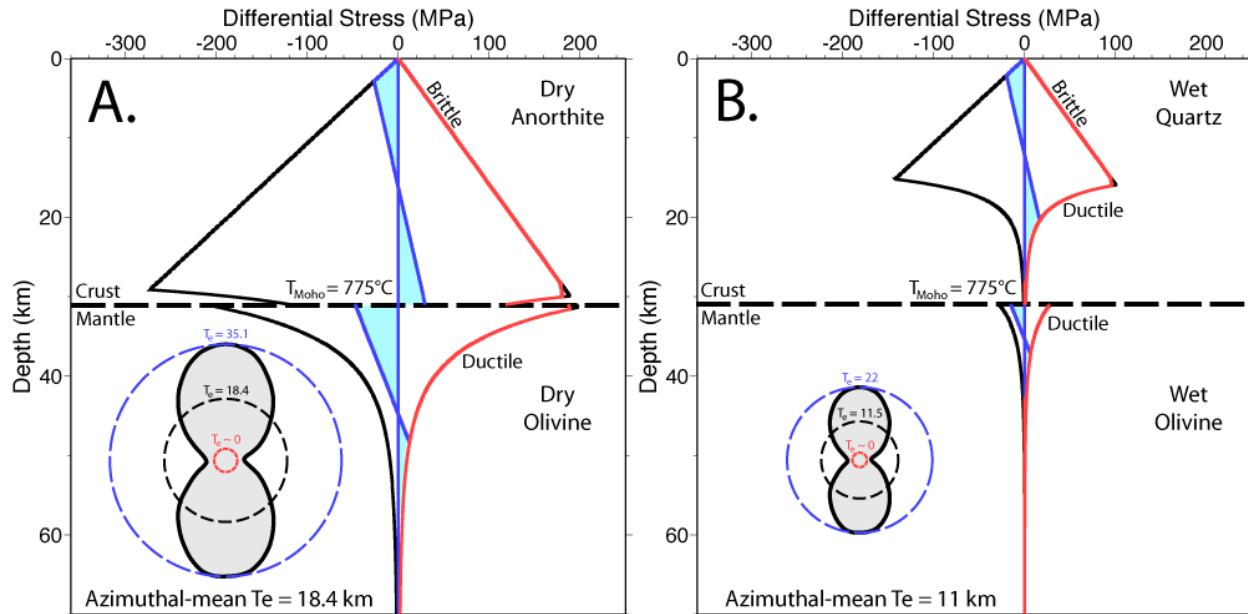


**Figure 10.** End-member yield strength envelopes (solid black lines) for the Basin and Range near the GPS sites, calculated using flow law parameters from measurements compiled in *Bürgmann and Dresen* [2008]. We assumed 1 mm grain size, strain rate  $10^{-14} \text{ s}^{-1}$  and friction coefficient  $\mu = 0.2$ . Fiber stress (blue lines) and moment integration area (cyan) used for modeling of effective elastic thickness  $T_e$  are also shown. Insets show expected azimuthal variation given whole-lithospheric failure in an E-W extension direction (red). (a) Dry anorthite over dry olivine; assuming no reference tectonic stress, model  $T_e = 35.1$  km (directionally averaged  $T_e = 18.4$  km after accounting for anisotropy due to failure along the extensional principal axis). (b) Saturated wet quartz crust over wet olivine mantle; model  $T_e = 22.1$  km (directionally averaged  $T_e = 11.5$  km).

When crustal thickness and temperature are known, they can be combined with recent measurements of rheological flow parameters to generate yield strength envelopes. Using geotherm modeling after that of *Lowry and Pérez-Gussinyé* [2011], we show in Figure 10 examples that illustrate the significance of assumptions regarding crustal lithology and water content. If the lithospheric column is wet and quartz is present in the lower crust (Figure 10b), dislocation creep in the crust decouples mantle deformation from the surface, and uppermost mantle deformation is also in the dislocation creep regime. If however feldspar dominates lower-crustal flow and the lithosphere is dry, lower crustal flow will be negligible and the Moho is at or near the frictional regime.

There are additional recent observations, however, that illuminate questions of crustal lithology and water. Figure 11a shows lateral variation in bulk-crustal seismic velocity ratios,  $V_p/V_s$ , derived from receiver functions and gravity data [after *Lowry and Pérez-Gussinyé*, 2011].  $V_p/V_s$  is extremely sensitive to the presence of quartz (which has low  $V_p/V_s < 1.5$ ), so low velocity ratios indicate abundant quartz. Relatively undeformed lithospheric blocks in the U.S. Cordillera (including Siletzia, the Sierra Nevada-Great Valley block, and the Colorado Plateau) are quartz-poor; the Snake River plain (where contemporary deformation is negligible [*Payne et al.*, 2008])

and the stable continental interior east of the Cordillera similarly have high  $V_P/V_S$ . Conversely, deforming zones and locations of past orogens have low  $V_P/V_S$  indicating high concentrations of crustal quartz. The Basin and Range study area has among the lowest  $V_P/V_S$  in the conterminous United States, rivaled only by western U.S. granitic batholith provinces, the Rio Grande rift, and the Ouachita, Penokean and Appalachian orogenic belts.

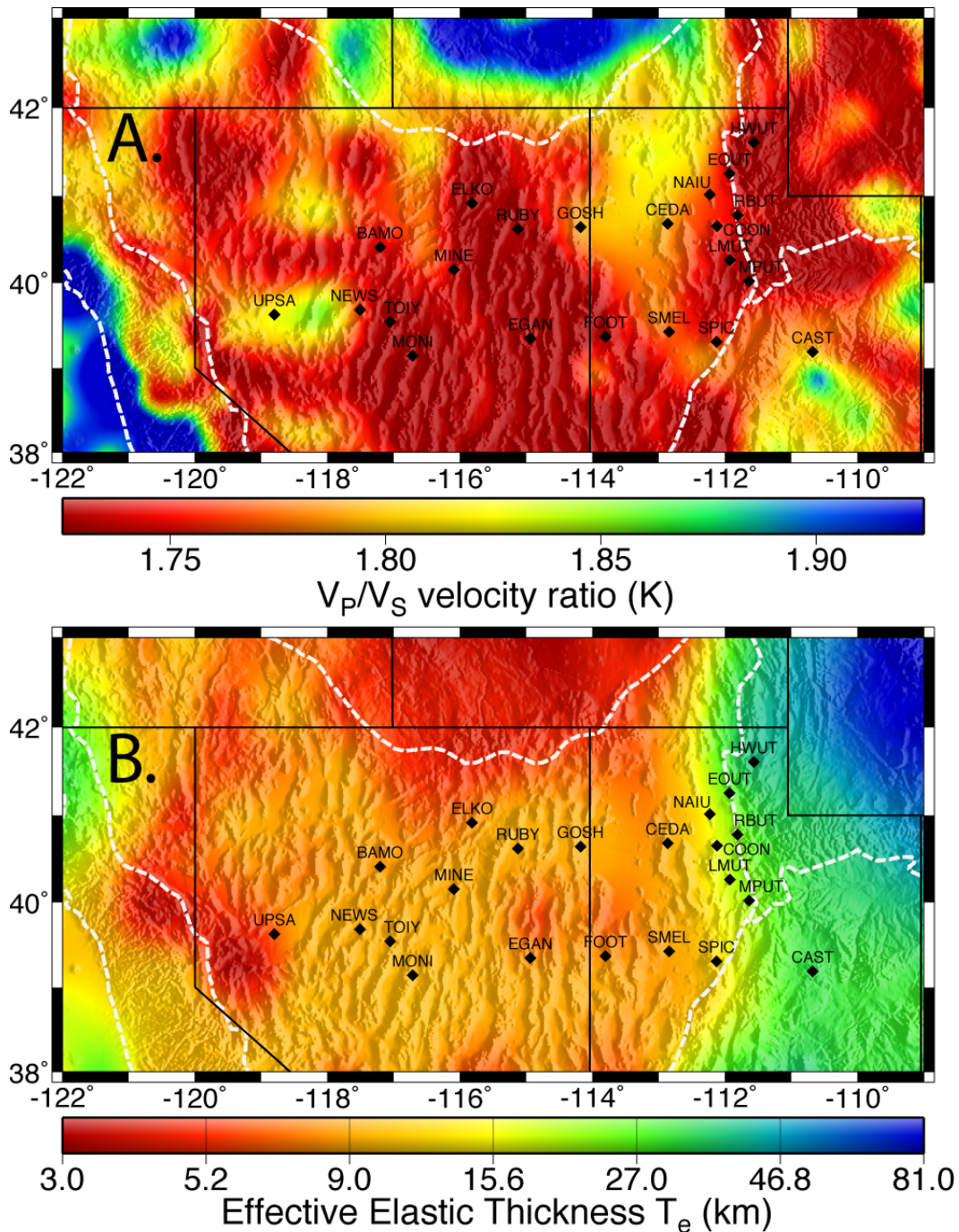


**Figure 11.** Measurements of (a) bulk-crustal  $V_P/V_S$  seismic velocity ratio and (b) effective elastic thickness  $T_e$ , after Lowry and Pérez-Gussinyé [2011].  $V_P/V_S$  reveals the study area to be among the most quartz-rich locations in the conterminous US;  $T_e$  within the network region is  $9.2 \pm 2.6$  km.

Another measurement that directly relates to rheology is the effective elastic thickness,  $T_e$ , of the lithosphere measured from relationships of gravity to topography (Figure 11b, after *Lowry and Pérez-Gussinyé* [2011]).  $T_e$  can be modeled to first order from yield strength envelopes like those shown in Figure 10 using relations described in *Lowry et al.* [2000]. Such modeling is complicated slightly in actively deforming zones because membrane (or “tectonic”) stress like that responsible for Basin and Range extension shifts the reference state of deviatoric stress from zero (where it is depicted with blue fiber stress in Figure 10) out into the limbs of the strength envelope [*Lowry and Smith*, 1995], thus reducing the remainder strength available to accommodate a perturbational stress fiber and hence support bending moment. The resulting directional dependence, or anisotropy, of  $T_e$  is commonly observed in spectral analyses [*Simons et al.*, 2000; *Kirby and Swain*, 2006; *Audet and Bürgmann*, 2011]. Here, we account for the anisotropy expected in an active rift zone by averaging the directional variation in  $T_e$  expected given a membrane stress at whole-lithospheric failure in one direction (i.e.,  $T_e$  near zero) and assuming no membrane stress in the orthogonal direction (i.e., the zero-reference state of stress depicted with blue fiber stress in Figure 10).

The directionally-averaged models using the end-member yield strength envelopes in Figure 10 are  $T_e = 18.4$  km for dry feldspar over dry olivine (Figure 10a), and  $T_e = 11.5$  km for wet quartz over wet olivine (Figure 10b). The average measured  $T_e$  within the Basin and Range portion of the GPS network is  $9.2 \pm 2.6$  km. The exceptionally low (near 1.7) crustal  $V_p/V_s$  coupled with low ( $< 10$  km)  $T_e$  in the Basin and Range thus implies that a wet quartz over wet olivine rheology is more likely than dry feldspar over dry olivine. *Wernicke et al.* [2008] based their inference of the latter in part on modeling studies of Pleistocene lake and postseismic rebound [*Bills et al.*, 2007; *Freed et al.*, 2007], but surface deformation on short timescales is notoriously insensitive to the presence or absence of lower crustal stress relaxation [*Nakiboglu and Lambeck*, 1983; *Willett et al.*, 1985; *A. Freed*, pers. comm. 2011]. Thus, the hypothesis of a Moho detachment surface is rendered unlikely by the combination of observations and models presented here.

### 6.6. Possible depth of frictional slip

Slow slip events and associated tectonic tremor in subduction zones often locates very near the frictional transition from velocity-weakening (“stick-slip”) to velocity-strengthening (“stable sliding”) as evidenced by their association with the base of interseismic frictional coupling and the bottom of seismic rupture in large earthquake events [*Lowry*, 2006; *Ide et al.*, 2007; *McCaffrey et al.*, 2008; *Chapman and Melbourne*, 2010]. The maximum rupture depth of Basin and Range earthquakes is  $\sim 15$  km [*Doser and Smith*, 1989], bolstering the interpretation of slip on a detachment surface at mid-crustal depths, as modeled and depicted in Figures 8-9. Rate- and state-dependent frictional slip models suggest frictional slip is exceptionally sensitive to small changes in ambient stress near the stability transition where frictional parameters ( $a - b$ )  $\sim 0$  [*Lowry*, 2006; *Liu and Rice*, 2007; *Perfettini and Ampuero*, 2008]. The inference of a strong frictional slip sensitivity is further supported by observations that deformation during subduction zone transients is perturbed by very small stresses associated with tidal and other loading phenomena [*Hawthorne and Rubin*, 2010; *Pollitz et al.*, 2013].

The base of the seismogenic layer is not the only possibility however. Slow slip events are also observed at shallow depths in subduction zones, including offshore of Nicoya Peninsula, Costa Rica [*Protti et al.*, 2003; *Outerbridge et al.*, 2010] and the Gisborne events in New Zealand [*McCaffrey et al.*, 2008; *Wallace and Eberhart-Phillips*, 2013]. These occur at depths more

consistent with the shallow frictional transition from (near-surface) stable to (deeper) stick-slip at about 150°C [e.g., *Moore and Saffer*, 2001]. Shallow low-angle normal faults have been identified in seismic data at many locations [e.g., *Smith and Bruhn*, 1984; *Gans et al.*, 1985; *Wernicke*, 1995], and in some instances surficial range-bounding fault scarps sole into these [e.g., *Axen et al.*, 1999]. *Hreinsdóttir and Bennett* [2009] found that a shallow low-angle normal fault in Italy is actively slipping at depths below 4 km, opening up the possibility that the source of Basin and Range transient deformation could be slip events near the top of the seismogenic zone rather than at the base.

### **6.7. Implied stress interaction and stress sensitivity**

Slip on detachment surfaces at mid-crustal or shallower depths resolves some inconsistencies between Basin and Range transient deformation versus the phenomenon observed in subduction zones and elsewhere. However a shallower source creates other problems. GPS site cross-correlations in Figure 7d suggest the transient deformation spans a more-than 500 km distance from UPSA on the west side of the Basin and Range to at least CEDA and SMEL. Neither seismic imaging nor structural evidence would support a mid-crustal detachment spanning that distance. There is ample evidence to suggest the presence of several smaller (50+ km wide) discontinuous detachments in the Basin and Range, however, including field observations of low-angle normal faults exhumed from mid-crustal depths [e.g., *Wernicke*, 1981; 1992; *Miller et al.*, 1983] and reflection seismic profiles of similar structures at depths of a few km [e.g., *Smith and Bruhn*, 1984; *Allmendinger et al.*, 1987]. Simultaneous activation of these faults would require some sort of stress interaction, in which strain induced by slip on one detachment fault would excite slip on neighboring low-angle normal faults.

The somewhat patchy distribution of slip in Figures 8-9 would be consistent with slip on multiple separate fault surfaces, but the slip inversion is highly underdetermined, so those models would change significantly with a different choice of regularization and constraints. Still, the raw GPS data also exhibit variations consistent with slip on multiple discontinuous surfaces. For example, in Figure 8a, sites GOSH, FOOT & CEDA in the central part of the network have very small transient displacements, whereas sites to both east and west exhibit significant ENE motion.

Changes in slip rate in response to small changes in stress would imply exceedingly high sensitivity to small stress perturbations (of order hundreds of Pa), which has also been inferred on subduction megathrusts [*Shen et al.*, 2004; *Lowry*, 2006; *Hawthorne and Rubin*, 2010; *Pollitz et al.*, 2013]. A robust slip/stress transfer function is also suggested by the fact that both the 2000.4 and 2004.4 events exhibited northward displacements while their eastward displacements were in opposite directions.

Rate- and state-dependent friction is not the only possible means by which to introduce nonlinearity in the relationship of stress forcing to strain, however. *Lavier et al.* [2013] propose that low-viscosity material in fracture networks within a higher-viscosity shear zone near the brittle-ductile transition could behave as a damped harmonic oscillator, which given optimal conditions of relative viscosities and thicknesses could generate creep events with durations and recurrence intervals spanning a broad range of timescales. This mechanism would generate events at mid-crustal depths just a few km deeper than those we infer, but it suffers some of the same limitations as rate-state frictional models in explaining Basin and Range transient deformation: Namely, it is difficult to imagine a process by which fracture networks might link

up over scales of ~500 km to facilitate event propagation on those scales. Hence, stress interaction would be required to explain the displacement behavior, implying high sensitivity of creep events to ambient stress perturbations.

## 7. Conclusions

Time-dependent displacements in the ~fifteen-year time series of GPS positions at twenty-two sites in the Basin and Range are dominated by a combination of elastic Earth response to hydrologic loading and several long-timescale (2–4 years) transient events. Subtracting estimates of hydrologic loading from climatological land-surface models plus one-year and half-year sinusoidal terms significantly reduces RMS residuals of the time series. Inspection of the climate model estimates at interannual timescales suggests no strong relationship to the transients, which have displacement directions and temporal dependence consistent with large-scale slow slip events on megadetachments.

Transient tectonic displacements in ~2000.4 and ~2004.4 are widespread, with movements in similar directions occurring in both eastern and western parts of the northern Basin and Range province. Cross-correlation analyses suggest that motions are most coherent in the west, between UPSA in the Walker Lane belt and SMEL ~100 km from the Wasatch fault, but sites throughout the region behave similarly. Most sites displaced eastward in the ~2000.4 event and westward in the ~2004.4 event, but displacements were northward during both events. The latter observation suggests strong sensitivity of slip to stress similar to that observed in slow slip events in other tectonic environments.

Previous studies interpreted Basin and Range transients as evidence of slow slip on a Moho detachment fault. Sparse GPS sampling in the Basin and Range coupled with low signal-to-noise ratio of the vertical displacements preclude estimation of the depth of the deformation source from GPS data alone, but frictional slip at the Moho would require a quartz-poor lower crust and anhydrous upper mantle. Extremely low (~1.7) crustal  $V_p/V_s$  and rheological modeling of low ( $9.2 \pm 2.6$  km) effective elastic thickness indicate that neither of these preconditions is likely in the northern Basin and Range. Instead, we propose slip on low-angle normal faults in the midcrust, near the ~15 km maximum focal depth of Basin and Range earthquakes, consistent with localization of slow slip events near the bottom of the seismogenic zone observed in other tectonic environments. Evidence for a single contiguous midcrustal detachment is lacking however, implicating a role for large-scale stress transfer across discontinuous faults.

## Acknowledgements

This manuscript was improved by comments of Rick Bennett and an anonymous reviewer. AC thanks the Indo-US Science and Technology Forum, New Delhi, India for financial support in the form of an Indo-US research fellowship. The efforts of ARL were supported by NSF grant EAR-0955909 and a Wilford Gardner travel award. GPS time series modeled here are from the Scripps Orbit and Permanent Array Center (SOPAC) MEaSURES data archive [Bock and Webb, 2012], using sites installed and maintained for the Basin and Range GEodetic Network (BARGEN) [Wernicke *et al.*, 2000] and University of Utah GPS Network [Puskas *et al.*, 2007] with technical support from the University Navstar Consortium (UNAVCO). The hydrologic land-surface models used in this study were acquired as part of the mission of NASA's Earth Science Division and archived and distributed by the Goddard Earth Sciences (GES) Data and Information Services Center (DISC) [Rodell *et al.*, 2004].

## References

- Audet, P., and R. Bürgmann (2011), Dominant role of tectonic inheritance in supercontinent cycles, *Nat. Geosci.*, 4(3), 184-187.
- Allmendinger, R. W., T. A. Hauge, E. C. Hauser, C. J. Potter, S. L. Klemperer, K. D. Nelson, P. Kneupfer, and J. Oliver (1987), Overview of the COCORP 40 N transect, western United States: The fabric of an orogenic belt, *Geol. Soc. Am. Bull.*, 98(3), 308-319.
- Axen, G. J., W. J. Taylor, and J. M. Bartley (1993), Space-time patterns and tectonic controls of Tertiary extension and magmatism in the Great Basin of the western United States, *Geol. Soc. Am. Bull.*, 105(1), 56-76.
- Axen, G. J., J. M. Fletcher, E. Cowgill, M. Murphy, P. Kapp, I. MacMillan, E. Ramos-Velázquez, and J. Aranda-Gómez (1999), Range-front fault scarps of the Sierra El Mayor, Baja California: Formed above an active low-angle normal fault? *Geology*, 27(3), 247-250.
- Behr, W. M., and J. P. Platt (2011), A naturally constrained stress profile through the middle crust in an extensional terrane, *Earth Planet. Sci. Lett.*, 303(3-4), 181-192, doi:10.1016/j.epsl.2010.11.044.
- Bennett, R. A. (2008), Instantaneous deformation from continuous GPS: Contributions from quasi-periodic loads, *Geophys. J. Int.*, 174(3), 1052-1064.
- Bennett, R. A., B. P. Wernicke, N. A. Niemi, A. M. Friedrich, and J. L. Davis (2003), Contemporary strain rates in the northern Basin and Range province from GPS data, *Tectonics*, 22(2), 1008, doi:10.1029/2001TC001355.
- Berglund, H. T., A. F. Sheehan, M. H. Murray, M. Roy, A. R. Lowry, R. S. Nerem, and F. Blume (2012), Distributed deformation across the Rio Grande Rift, Great Plains and Colorado Plateau, *Geology*, 40(1), 23-26.
- Bills, B. G., K. D. Adams, and S. G. Wesnousky (2007), Viscosity structure of the crust and upper mantle in western Nevada from isostatic rebound patterns of the late Pleistocene Lake Lahontan high shoreline, *J. Geophys. Res.*, 112(B6), doi:10.1029/2005JB003941.
- Bock, Y. and F. H. Webb (2012), MEASUREs Solid Earth Science ESDR System, [sopac.ucsd.edu](http://sopac.ucsd.edu), accessed July 2012. Digital media.
- Brooks, B. A., J. Foster, D. Sandwell, C. J. Wolfe, P. Okubo, M. Poland, and D. Myer (2008), Magmatically triggered slow slip at Kilauea volcano, Hawaii, *Science*, 321(5893), 1177-1177, doi: 10.1126/science.1159007.
- Brudzinski, M., E. Cabral-Cano, F. Correa-Mora, C. DeMets, and B. Márquez-Azúa (2007), Slow slip transients along the Oaxaca subduction segment from 1993-2007, *Geophys. J. Int.*, 171, 523-538, doi:10.1111/j.1365-246X.2007.03542.x.
- Bürgmann, R., and G. Dresen (2008), Rheology of the lower crust and upper mantle: Evidence from rock mechanics, geodesy, and field observations, *Annu. Rev. Earth Planet. Sci.*, 36, 531-567.
- Buehler, J. S., and P. M. Shearer (2010),  $P_n$  tomography of the western United States using USArray, *J. Geophys. Res.*, 115(B9), 1978-2012.
- Cervelli, P., P. Segall, K. Johnson, M. Lisowski, and A. Miklius (2002), Sudden aseismic fault slip on the south flank of Kilauea volcano, *Nature*, 415(6875), 1014-1018 doi: 10.1038/4151014a.
- Chapman, J. S., and T. I. Melbourne (2009), Future Cascadia megathrust rupture delineated by episodic tremor and slip, *J. Geophys. Res.*, 36, #L22301, doi:10.1029/2009GL040465.

- Colgan, J. P., T.A. Dumitru, P. W. Reiners, J. L. Wooden, and E. L. Miller (2006), Cenozoic tectonic evolution of the basin and range province in northwestern Nevada, *Am. J. Sci.*, 306(8), 616–654, doi:10.2475/08.2006.023.
- Davis, G. A., and G. S. Lister (1988), Detachment faulting in continental extension; Perspectives from the southwestern US Cordillera, *Geol. Soc. Am. Spec. Pap.*, 218, 133-160.
- Davis, J. L., B. P. Wernicke, S. Bisnath, N. A. Niemi, and P. Elósegui (2006), Subcontinental-scale crustal velocity changes along the Pacific-North America plate boundary, *Nature*, 441, 1131–1134, doi:10.1038/nature04781.
- Dilles, J. H., and P. B. Gans (1995), The chronology of Cenozoic volcanism and deformation in the Yerington area, western Basin and Range and Walker Lane, *Geol. Soc. Am. Bull.*, 107(4), 474-486.
- Dixon, J. E., T. H. Dixon, D. R. Bell, and R. Malservisi (2004), Lateral variation in upper mantle viscosity: Role of water, *Earth Planet. Sci. Lett.*, 222(2), 451-467.
- Dong, D., P. Fang, Y. Bock, M. K. Cheng, and S. Miyazaki (2002), Anatomy of apparent seasonal variations from GPS-derived site position time series, *J. Geophys. Res.*, 107(B4), doi:10.1029/2001JB000573.
- Doser, D. I., and R. B. Smith (1989), An assessment of source parameters of earthquakes in the Cordillera of the western United States, *Bull. Seismol. Soc. Am.*, 79(5), 1383-1409.
- Dragert, H., K. Wang, and T. S. James (2001), A silent slip event on the deeper Cascadia subduction interface, *Science* 292, 1525–1528.
- Dziewonski, A. M., and D. L. Anderson (1981), Preliminary reference Earth model, *Phys. Earth Planet. Inter.*, 25(4), 297–356.
- Elósegui, P., J. L. Davis, J. X. Mitrovica, R. A. Bennett, and B. P. Wernicke (2003), Crustal loading near Great Salt Lake, Utah, *Geophys. Res. Lett.*, 30(3), doi:10.1029/2002GL016579.
- Farrell, W. E. (1972), Deformation of Earth by surface loads, *Rev. Geophys. Space Phys.*, 10(3), 761–797, doi: 10.1029/RG010i003p00761.
- Freed, A. M., R. Bürgmann, and T. Herring (2007), Far-reaching transient motions after Mojave earthquakes require broad mantle flow beneath a strong crust, *Geophys. Res. Lett.*, 34(19), L19302.
- Foster, J. H., A. R. Lowry, and B. A. Brooks, Fault frictional parameters and material properties revealed by slow slip at Kilauea volcano, Hawai'i, *Geophys. Res. Lett.*, 40(23), 6059-6063.
- Gans, P. B., E. L. Miller, J. McCarthy, and M. L. Ouldcott (1985), Tertiary extensional faulting and evolving ductile-brittle transition zones in the northern Snake Range and vicinity: New insights from seismic data, *Geology*, 13(3), 189-193.
- Hammond, W. C., and W. Thatcher (2004), Contemporary tectonic deformation of the Basin and Range province, western United States: 10 years of observation with the Global Positioning System, *J. Geophys. Res.*, 109(B8), #B08403, doi:10.1029/2003JB002746.
- Hauser, E., et al. (1987), Crustal structure of eastern Nevada from COCORP deep seismic reflection data, *Geol. Soc. Am. Bull.*, 99, 833-844.
- Hawthorne, J. C., and A. M. Rubin (2010), Tidal modulation of slow slip in Cascadia, *J. Geophys. Res.*, 115(B9), #B09406.
- Hirose, H., K. Hirahara, F. Kimata, N. Fujii, and S. Miyazaki (1999), A slow thrust slip event following the two 1996 Hyuganada earthquakes beneath the Bungo Channel, southwest Japan, *Geophys. Res. Lett.* 26, 3237–3240.

- Howard, K. A., and B. E. John (1987), Crustal extension along a rooted system of imbricate low-angle faults: Colorado River extensional corridor, California and Arizona, *Geol. Soc. London Spec. Pub.*, 28(1), 299-311.
- Hreinsdóttir, S., and R. A. Bennett (2009), Active aseismic creep on the Alto Tiberina low-angle normal fault, Italy, *Geology*, 37(8), 683-686.
- Ide, S., G. C. Beroza, D. R. Shelly, and T. Uchide (2007), A scaling law for slow earthquakes. *Nature*, 447(7140), 76-79.
- Kirby, J. F., and C. J. Swain (2006), Mapping the mechanical anisotropy of the lithosphere using a 2D wavelet coherence, and its application to Australia, *Phys. Earth Planet. Int.*, 158(2), 122-138.
- Klemperer, S. L., T. A. Hauge, E. C. Hauser, J. E. Oliver, and C. J. Potter (1986), The Moho in the northern Basin and Range Province, Nevada, along the COCORP 40 degrees N seismic-reflection transect, *Geol. Soc. Am. Bull.*, 97, 603-618.
- Larson, K. M., A. R. Lowry, V. Kostoglodov, W. Hutton, O. Sánchez, K. Hudnut, and G. Suárez (2004), Crustal deformation measurements in Guerrero, México, *J. Geophys. Res.*, 109(B4), B04409, doi:10.1029/2003JB002843.
- Lavier, L. L., R. A. Bennett, and R. Duddu (2013), Creep events at the brittle ductile transition, *Geochem. Geophys. Geosys.*, 14(9), 3334-3351.
- Linde, A. T., M. T. Gladwin, M. J. S. Johnston, R. L. Gwyther, and R. G. Bilham (1996), A slow earthquake sequence on the San Andreas fault, *Nature*, 383, 65-68.
- Lister, G. S., and G. A. Davis (1989), The origin of metamorphic core complexes and detachment faults formed during Tertiary continental extension in the northern Colorado River region, USA, *J. Struct. Geol.*, 11(1), 65-94.
- Liu, Y., and J. R. Rice (2007), Spontaneous and triggered aseismic deformation transients in a subduction fault model, *J. Geophys. Res.*, 112(B9).
- Lowry, A. R. (2006), Resonant slow fault slip in subduction zones forced by climatic load stress, *Nature*, 442(7104), 802-805, doi:10.1038/nature05055.
- Lowry, A. R., and M. Pérez-Gussinyé (2011), The role of crustal quartz in controlling Cordilleran deformation, *Nature*, 471(7338), 353-357.
- Lowry, A. R., and R. B. Smith (1995), Strength and rheology of the western US Cordillera, *J. Geophys. Res.*, 100(B9), 17,947-17,963.
- Lowry, A. R., N. M. Ribe, and R. B. Smith (2000), Dynamic elevation of the Cordillera, western United States, *J. Geophys. Res.*, 105, 23,371-23,390.
- Lowry, A.R., K.M. Larson, V. Kostoglodov, and R.G. Bilham (2001), Transient fault slip in Guerrero, southern Mexico, *Geophys. Res. Lett.*, 28, 3753-3756.
- McCaffrey, R., L. M. Wallace, and J. Beavan (2008), Slow slip and frictional transition at low temperature at the Hikurangi subduction zone, *Nat. Geosci.*, 1(5), 316-320, doi:10.1038/ngeo178.
- Miller, E. L., P. B. Gans, and J. Garing (1983), The Snake Range decollement: An exhumed mid-Tertiary ductile-brittle transition, *Tectonics*, 2(3), 239-263.
- Moore, J. C., and D. Saffer (2001), Updip limit of the seismogenic zone beneath the accretionary prism of southwest Japan: An effect of diagenetic to low-grade metamorphic processes and increasing effective stress, *Geology*, 29(2), 183-186.
- Nakiboglu, S. M., and K. Lambeck (1983), A reevaluation of the isostatic rebound of Lake Bonneville, *J. Geophys. Res.*, 88(B12), 10,439-10,447.

- Nadeau, R.M., and D. Dolenc (2005), Nonvolcanic tremors deep beneath the San Andreas fault, *Science*, 307(5708), p389.
- Ohta, Y., J. T. Freymueller, S. Hreinsdottir, and H. Suito (2006), A large slow slip event and the depth of the seismogenic zone in the south central Alaska subduction zone, *Earth Planet. Sci. Lett.*, 247(1-2), 108–116, doi: 10.1016/j.epsl.2006.05.013.
- Outerbridge, K. C., T. H. Dixon, S. Y. Schwartz, J. I. Walter, M. Protti, V. Gonzalez, J. Biggs, M. Thorwart, and W. Rabbel, (2010), A tremor and slip event on the Cocos-Caribbean subduction zone as measured by a global positioning system (GPS) and seismic network on the Nicoya Peninsula, Costa Rica, *J. Geophys. Res.*, 115(B10), #B10408 doi: 10.1029/2009JB006845.
- Payne, S. J., R. McCaffrey, and R. W. King (2008), Strain rates and contemporary deformation in the Snake River Plain and surrounding Basin and Range from GPS and seismicity, *Geology*, 36(8), 647-650.
- Perfettini, H., and J. P. Ampuero (2008), Dynamics of a velocity strengthening fault region: Implications for slow earthquakes and postseismic slip, *J. Geophys. Res.*, 113(B9).
- Pollitz, F. F., A. Wech, H. Kao, and R. Bürgmann (2013), Annual modulation of non-volcanic tremor in northern Cascadia, *J. Geophys. Res.*, 118(B5), 2445-2459.
- Protti, M., V. González, T. Kato, T. Iinuma, S. Miyazaki, K. Obana, Y. Kaneda, P. La Femina, T. Dixon, and S. Schwartz (2004), A creep event on the shallow interface of the Nicoya Peninsula, Costa Rica seismogenic zone, *Eos Trans. Am. Geophys. Un. Fall Mtg. Abstr.*
- Puskas, C. M., R. B. Smith, C. M. Meertens, and W. L. Chang (2007), Crustal deformation of the Yellowstone–Snake River Plain volcanotectonic system: Campaign and continuous GPS observations, 1987–2004, *J. Geophys. Res.*, 112(B3), doi:10.1029/2006JB004325.
- Rodell, M., P. R. Houser, U. Jambor, J. Gottschalk, K. Mitchell, C. J. Meng, K. Arsenault, B. Cosgrove, J. Radakovich, M. Bosilovitch, J. K. Entin, J. P. Walker, D. Lohmann, and D. Toll (2004), The global land data assimilation system. *Bull. Am. Meteor. Soc.*, 85(3), 381-394.
- Schutt, D. L., A. R. Lowry, J. Buehler, and D. D. Blackwell (2013), Lithosphere temperatures within the western United States, abstract for the EarthScope National Meeting.
- Seunarine, L., and A. R. Lowry (2011), Constraining the dynamical behavior of the western US lithosphere through computational modeling: Evidence that lower crustal flow plays a significant role in load accommodation, Abstract #T23B-2389, AGU Fall Mtg, Dec 5-9, San Francisco CA.
- Shen, Z. K., Q. Wang, R. Bürgmann, Y. Wan, and J. Ning (2005), Pole-tide modulation of slow slip events at circum-Pacific subduction zones, *Bull. Seismol. Soc. Am.*, 95(5), 2009-2015.
- Simons, F. J., M. T. Zuber, and J. Korenaga (2000), Isostatic response of the Australian lithosphere: Estimation of effective elastic thickness and anisotropy using multitaper spectral analysis, *J. Geophys. Res.*, 105(B8), 19,163-19,184.
- Smith, K. D., D. von Seggern, G. Blewitt, L. Preston, J. G. Anderson, B. P. Wernicke, and J. L. Davis (2004), Evidence for deep magma injection beneath Lake Tahoe, Nevada-California, *Science*, 305, 1277-1280.
- Smith, R. B., and R. L. Bruhn (1984), Intraplate extensional tectonics of the eastern Basin–Range: Inferences on structural style from seismic reflection data, regional tectonics, and thermal–mechanical models of brittle–ductile deformation, *J. Geophys. Res.*, 89(B7), 5733-5762.

- Stockli, D. F., T. A. Dumitru, M. O. McWilliams, and K. A. Farley (2003), Cenozoic tectonic evolution of the White Mountains, California and Nevada, *Geol. Soc. Am. Bull.*, 115(7), 788–816, doi:10.1130/0016-7606.
- Wahr, J. M. (1983), Computing tides, nutations and tidally induced variations in the Earth's rotation rate for a rotating, elliptical Earth, in *Geodesy and Global Geodynamics*, edited by H. Moritz & H. Sunkel, 327–380.
- Wallace, L. M., and D. Eberhart-Phillips (2013), Newly observed, deep slow slip events at the central Hikurangi margin, New Zealand: Implications for downdip variability of slow slip and tremor, and relationship to seismic structure, *Geophys. Res. Lett.*, 40(20), 5393-5398.
- Wdowinski, S., Y. Bock, J. Zhang, P. Fang, and J. Genrich (1997), Southern California Permanent GPS Geodetic Array: Spatial filtering of daily positions for estimating coseismic and postseismic displacements induced by the 1992 Landers earthquake, *J. Geophys. Res.*, 102(B8), 18,057-18,070.
- Wech, A.G., C. M. Boese, T. A. Stern, and J. Townend (2012), Tectonic tremor and deep slow slip on the Alpine Fault, *Geophys. Res. Lett.*, 39(10), doi:10.1029/2012GL051751.
- Wernicke, B. (1981), Low-angle normal faults in the Basin and Range province: Nappe tectonics in an extending orogen, *Nature*, 291, 645-648.
- Wernicke, B. (1992), Cenozoic extensional tectonics of the Cordillera, U.S., in *The Cordilleran Orogen; Conterminous U.S.*, edited by B. C. Burchfiel, P. W. Lipman, and M. L. Zoback, pp. 553 – 582, *Geol. Soc. of Am.*, Boulder, Colo.
- Wernicke, B. (1995), Low-angle normal faults and seismicity: A review, *J. Geophys. Res.*, 100(B10), 20159-20174.
- Wernicke, B, A. M. Friedrich, N. A. Niemi, R. A. Bennett, and J. L. Davis (2000), Dynamics of plate boundary fault systems from the Basin and Range Geodetic Network (BARGEN) and geologic data, *Geol. Soc. Am. Today*, 10(11), 1-7.
- Wernicke, B., J. L. Davis, N. A. Niemi, P. Luffi, and S. Bisnath (2008), Active megadetachment beneath the western United States, *J. Geophys. Res.*, 113, #B11409, doi:10.1029/2007JB005375.
- Wernicke, B., and J. L. Davis (2010), Detecting large-scale intracontinental slow-slip events (SSEs) using geodograms, *Seismol. Res. Lett.*, 81(5).
- Willett, S. D., D. S. Chapman, and H. J. Neugebauer (1985), A thermo-mechanical model of continental lithosphere, *Nature*, 314, 520-523.